

**Tropospheric Delay Modelling at Radio Wavelengths
for Space Geodetic Techniques**

Johannes Böhm

Veröffentlichung
des Instituts für Geodäsie und Geophysik

2007

Published by the Institutes of the Course on 'Geodesy and Geoinformation'
of the Vienna University of Technology
Gußhausstraße 27-29
A-1040 Wien

Responsible for this Issue: Johannes Böhm
Printed by: Grafisches Zentrum

This issue was submitted as Habilitation Thesis at the Vienna University of Technology.

Diese Arbeit wurde an der Technischen Universität Wien als Habilitationsschrift eingereicht.

Auflage: 100 Stück

ISSN 1811-8380

Contents

Introduction	iv
<u>Paper A:</u>	<u>1</u>
J. Böhm and H. Schuh, Vienna mapping functions in VLBI analyses, <i>Geophysical Research Letters</i> , Vol. 31, L01603, doi:10.1029/2003GL018984, 2004.	
<u>Paper B:</u>	<u>13</u>
J. Böhm, B. Werl, and H. Schuh, Troposphere mapping functions for GPS and VLBI from ECMWF operational analysis data, <i>Journal of Geophysical Research</i> , Vol. 111, B02406, doi:10.1029/2005JB003629, 2006a.	
<u>Paper C:</u>	<u>35</u>
J. Böhm, A. Niell, P. Tregoning, and H. Schuh, Global Mapping Function (GMF): A new empirical mapping function based on numerical weather model data, <i>Geophysical Research Letters</i> , Vol. 33, L07304, doi:10.1029/2005GL02554, 2006b.	
<u>Paper D:</u>	<u>47</u>
J. Böhm, R. Heinkelmann, and H. Schuh, Short Note: A Global Model of Pressure and Temperature for Geodetic Applications, <i>Journal of Geodesy</i> , doi:10.1007/s00190-007-0135-3, 2007a.	
<u>Paper E:</u>	<u>57</u>
J. Böhm, P.J. Mendes Cerveira, H. Schuh, and P. Tregoning, The impact of mapping functions for the neutral atmosphere based on numerical weather models in GPS data analysis, <i>IAG Symposium Series</i> , Vol. 130, Springer-Verlag, edited by Paul Tregoning and Chris Rizos, pp 837-843, 2007b.	
<u>Paper F:</u>	<u>69</u>
J. Böhm and H. Schuh, Troposphere Gradients from the ECMWF in VLBI analysis, <i>Journal of Geodesy</i> , Vol. 81, No. 6-8, pp 409-421, doi:10.1007/s00190-006-0126-9, 2007c.	
Appendix	

Introduction

Modelling tropospheric delays for space geodetic techniques observing at radio wavelengths has been the author's major research area over the last years. These techniques are the Global Positioning System (GPS) of the United States of America, the Global Navigation Satellite System (GLONASS) as the Russian counterpart, the French system DORIS (Doppler Orbitography and Radiopositioning Integrated by Satellite) with transmitting antennas at the stations, and Very Long Baseline Interferometry (VLBI) observing signals from extragalactic radio sources. Tropospheric delays, i.e., the delays in the neutral atmosphere, amount to about 2.3 m in zenith direction for stations at sea level and can be as large as 23 m for observations at 5° elevation. Proper modelling of these delays is critical for the accuracy of space geodetic techniques because any imperfection of these models affects the accuracy of geodetic parameters, e.g., station coordinates and velocities realizing the Terrestrial Reference Frame (TRF). In particular, errors of the station height component can be directly related to a mismodelled tropospheric delay. A stable and highly accurate TRF is essential for many investigations w.r.t. global change, like sea level rise. The challenging goals for the Global Geodetic Observing System (GGOS) of the International Association of Geodesy (IAG) are an accuracy of 1 mm for positions and 0.1 mm/year for velocities of hundreds of globally distributed observing stations over decadal time periods.

Tropospheric delays are usually separated into a hydrostatic and a wet part. Each part is represented as a product of the delay in zenith direction and the corresponding hydrostatic or wet mapping function. These mapping functions project the zenith delay to the elevation angle of the observation, and use continued fraction forms with three coefficients ('a', 'b', and 'c'). The hydrostatic zenith delays can be determined very accurately from pressure values observed at the sites, whereas the wet zenith delays are estimated in the analysis of the space geodetic observations by using the wet mapping function as partial derivative. A thorough multi-technique comparison of tropospheric zenith delays is provided by Snajdrova et al. (2005). The abstract of this paper can be found in the Appendix.

Until a few years ago, the NMF (Niell Mapping Functions) were mainly used in the software packages. These mapping functions have been derived from a standard atmosphere model, and have been validated with radiosonde data primarily available in the northern hemisphere. The NMF are given at five distinct latitude bands, are symmetric with respect to the equator

(apart from a phase shift of half a year for the different seasons), and do only contain an annual signal.

It was again Arthur Niell who first presented mapping functions that are based on data from a global Numerical Weather Model (NWM) with a temporal resolution of 6 hours, i.e., the Isobaric Mapping Functions (IMF). Whereas the hydrostatic IMF uses the height of the 200 hPa pressure level, the wet IMF is based on a coarse raytrace at 3.3° elevation through the pressure levels provided with the NWM. This approach induced the author to adopt a rigorous raytrace at 3.3° elevation for both, the hydrostatic and wet mapping function, naming it VMF (Vienna Mapping Functions) (Paper A: Böhm and Schuh 2004).

Whereas the coefficients 'a' of the continued fraction form are determined from the raytrace, the 'b' and 'c' coefficients of the VMF are still determined from empirical equations using station latitude and the day of the year (doy) as input parameters. The coefficients 'b' and 'c' are symmetric with respect to the equator. A closer look at the Antarctica, however, revealed that symmetric 'b' and 'c' coefficients are not sufficient there, because the properties of the mapping functions at the South Pole differ significantly from those at the North Pole. This led to the development of the VMF1 (Vienna Mapping Functions 1), which are based on new 'b' and 'c' coefficients (Paper B: Böhm et al. 2006a). Comparisons with radiosonde data by Arthur Niell showed that the precision in terms of station height is ± 3 mm for the VMF1 compared to more than ± 1 cm for the NMF.

Comparisons between the NMF and the VMF1, using the techniques NMF and VMF1, showed systematic differences causing large station height changes of more than 1 cm, especially over the Antarctica but also around East Asia (Eastern China and Japan). Since the implementation of the VMF1 required major changes of the software packages, some developers were asking for a mapping function as easy to implement as the NMF, but consistent with the VMF1 over longer time scales. Thus, the GMF (Global Mapping Functions) (Paper C: Böhm et al. 2006b) which are based on spherical harmonics up to degree and order 9 have been developed. For the determination of the TRF, the GMF yield approximately the same results as the VMF1 given at 6 hours time intervals, although in terms of precision they are not more precise than the NMF. The reason for the latter is that GMF and NMF only account for the annual variation and not for large weather changes at synoptic time scales.

If pressure values are not available for the sites neither from a local pressure sensor nor from a NWM, then simple models assuming 1013.25 hPa at sea level have been used so far to determine the hydrostatic zenith delays. These models have significant deficiencies, especially over the Antarctica, and lead to large station height errors. Consequently, the model GPT (Global Pressure and Temperature) (Paper D: Böhm et al. 2007a) has been developed. Similar to GMF it uses spherical harmonics up to degree and order 9.

Many GPS and VLBI analyses have been carried out with VMF1, GMF, and GPT, not only by the author himself but also by other groups. These investigations confirm the significant height changes with the new models as well as the improvement in precision with VMF1 compared to NMF. A paper that was chosen exemplarily here is about a GPS analysis of globally distributed stations using the software package GAMIT/GLOBK with NMF, VMF1, and GMF (Paper E: Böhm et al. 2007b). The abstract of a very detailed VLBI analysis (Tesmer et al. 2007) is added to the Appendix.

All mapping functions mentioned above only depend on the elevation angle but not on the azimuth of the observation, although the azimuthal asymmetry can be as large as a few decimeters at 5° elevation and thus should not be ignored. Usually, horizontal north and east gradients are estimated within the analysis, but it would be preferable to get this information from NWM, too. A two-dimensional approach has been carried out (Paper F: Böhm and Schuh 2007c) to derive hydrostatic and wet gradients from a NWM for all VLBI and International Global Navigation Satellite Systems (GNSS) Service (IGS) stations. Nevertheless, future investigations are necessary to improve these gradients or – if the accuracy of the NWM permits – direct raytracing could be applied to get the delay for each observation.

VMF1 together with observed pressure values as well as the combination GMF/GPT have proven to be essential contributions to the analysis of space geodetic techniques observing at radio wavelengths. Now, most GNSS and VLBI analysis software packages used by analysis groups all over the world include these models. Consequently, the most recent IERS Conventions (update from 28 June 2007, <http://tai.bipm.org/iers/convupdt/convupdt.html>) recommend the use of the VMF1 or – if VMF1 is still not available – the combination GPT with GMF. All necessary data (time series with VMF1 and a priori hydrostatic zenith delays for VLBI stations since 1979, global 2.5° x 2.0° grids with VMF1 and hydrostatic zenith

delays since 1994 – both determined from data of the European Centre for Medium-Range Weather Forecasts ECMWF) as well as the Fortran source code for VMF1, GMF, and GPT can be found at the webpage <http://www.hg.tuwien.ac.at/~ecmwfl>. It is also planned to augment these time series with forecasting data so that VMF1 can be used for real-time applications.

Future investigations will focus on the improvement of tropospheric parameter estimation by the use of turbulence theory. Wind speed as well as information about the wet troposphere above the site can be derived from NWM to gain information about the wet delays and their covariances in space and time. As already introduced several years ago (Appendix: Böhm and Schuh 2001) spherical harmonics will be applied to extend the traditional combination of mapping functions and gradients. This approach will be particularly valuable, if future VLBI systems allow for a significantly larger number of observations.

Acknowledgements

I would like to thank Harald Schuh and all members of the Research Group 'Advanced Geodesy' of the Institute of Geodesy and Geophysics for the excellent cooperation and many fruitful discussions. It is the inspiring atmosphere within the group that has made this work possible.

Greatly acknowledged is the Austrian Weather Service (Zentralanstalt für Meteorologie und Geodynamik ZAMG) for providing access to the data of the European Centre for Medium-Range Weather Forecasts (ECMWF).

I also want to express my thanks to Arthur Niell whose work was the basis for many ideas and who has been giving me a lot of valuable advices to improve the models. I also like to acknowledge numerous other colleagues all over the world for the excellent cooperation over the last years.

The International VLBI Service (IVS) and the International GNSS Service (IGS) are acknowledged for providing free access to the observational data.

Thanks to the Austrian Science Fund (FWF) for supporting parts of the work presented here within projects P16992-N10 and P18404-N10.

Johannes Böhm and Harald Schuh

Vienna mapping functions in VLBI analyses

Geophysical Research Letters

Vol. 31, L01603, doi:10.1029/2003GL018984

2004

Vienna Mapping Functions in VLBI Analyses

Johannes Böhm and Harald Schuh

Abstract

In the past few years, numerical weather models (NWM) have been investigated to improve mapping functions which are used for tropospheric delay modeling in VLBI and GPS data analyses. The Vienna Mapping Functions VMF are based on direct raytracing through NWM, and so they are able to exploit the full information provided in the NWM. On the other hand, the Isobaric Mapping Functions IMF are using intermediate parameters calculated from the NWM. In this study, pressure level data from ECMWF (European Centre for Medium-Range Weather Forecasts) are applied to determine the coefficients of the VMF and the IMF. Used for the analyses of IVS-R1 and IVS-R4 VLBI sessions, both mapping functions improve the repeatability of baseline lengths (by ~10% for IVS-R1 and ~5% for IVS-R4) compared to the Niell Mapping Functions NMF.

1 Introduction

Raytracing through radiosonde data has often been applied to develop and validate mapping functions which are needed for tropospheric modeling in VLBI and GPS data analyses. For example, the Niell Mapping Functions NMF [Niell, 1996], which require station height, station latitude and day of the year as input parameters, were developed using radiosonde data over a wide range of latitudes.

In recent years, much effort has been put into the development of mapping functions which are based on data from numerical weather models. Niell [2001] proposed the Isobaric Mapping Functions (IMF) which apply as input parameters the height of the 200 mbar pressure level ('z200') and the ratio of the wet path delay along a straight line at 3.3° elevation and its zenith delay ('smfw3'). The equations relating these two parameters to the coefficients of the continued fraction form (see eq. 1) are based on raytracing through radiosonde data. IMFh provides the information to allow correction for hydrostatic north-south and east-west gradients before estimating the remaining wet gradients.

When working on the implementation of these mapping functions with pressure level data from the ECMWF, it became evident that the NWM could be exploited more rigorously by

discarding intermediate parameters like z_{200} and $smfw3$. The main idea for the Vienna Mapping Functions VMF is to simply use the raytracing through the NWM directly instead of taking intermediate steps.

2 Determination of the Vienna Mapping Functions (VMF)

The continued fraction form [Marini, 1972] for the hydrostatic and wet mapping function for an elevation angle e is shown in eq. 1 [Herring, 1992]. This form is also used in the NMF [Niell, 1996] and in the IMF [Niell, 2001].

$$(1) \quad mf(e) = \frac{1 + \frac{a}{1 + \frac{b}{1 + c}}}{\sin e + \frac{a}{\sin e + \frac{b}{\sin e + c}}}$$

Three coefficients a , b and c are sufficient to map zenith delays down to elevations of 3° . In the case of VMF, these coefficients are determined from raytracing through NWM. A description of the raytracing can be found in *Boehm and Schuh* [2003]. Input parameters for the raytracing program are an initial elevation angle e_0 , and values for height, temperature and water vapor pressure at distinct pressure levels in the neutral atmosphere (e.g. 15 levels from 1000 to 10 hPa total pressure). The raytracing then yields the outgoing (vacuum) elevation angle e (see figure 1), and the values for the hydrostatic and the wet mapping function. The hydrostatic mapping function includes the geometric bending effect.

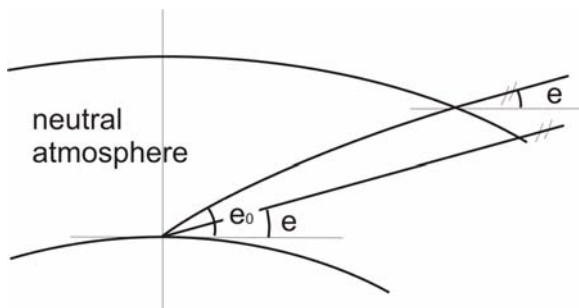


Figure 1. Bending of the ray in the neutral atmosphere. The outgoing (vacuum) elevation angle e is smaller than the initial elevation angle e_0 .

Two ways of determining the coefficients in eq. 1 from raytracing through ECMWF pressure levels will be presented here. The first one is rigorous, whereas the second one is faster and still of equivalent accuracy.

2.1 Rigorous determination of the coefficients: VMF(rig)

For each site (e.g. VLBI station) and each epoch when ECMWF pressure level data are available, i.e. every six hours, the hydrostatic [Davis *et al.*, 1985] and wet mapping functions as well as the outgoing (= vacuum) elevation angles are determined by raytracing through the pressure levels at ten different initial elevation angles (90°, 70°, 50°, 30°, 20°, 15°, 10°, 7°, 5°, 3.3°). Then, the coefficients a , b and c for the continued fraction form (eq. 1) for the hydrostatic and wet mapping function are estimated in a least-squares procedure. The adjustment shows that three coefficients are enough to map the zenith delays down to 3° elevation with residuals less than 2 mm. So, at each site time series of six parameters (a_h , b_h , c_h , a_w , b_w , c_w) are determined with a resolution of six hours. This approach is only used for test purposes, e.g. for the validation of the fast approach of VMF (see section 2.2).

2.2 Fast determination of the coefficient a: VMF(fast)

Although computers are very powerful and fast today, raytracing is still time consuming, especially if it has to be performed for many sites, several (e.g. four) times per day and ten times per grid point. For this reason, a fast version of the rigorous approach has been developed that yields similar values for the mapping functions [Boehm and Schuh, 2003] but is about ten times faster than VMF(rig). Instead of determining the raytracing at ten different elevation angles, the raytracing is only calculated for one initial elevation angle of 3.3°. This yields one value for the hydrostatic mapping function, one value for the wet mapping function, and the vacuum elevation angle ($\sim 3^\circ$). Then, pre-defined formulas are used for the b_h , c_h , b_w and c_w coefficients, and the coefficients a_h , a_w can be determined by simply inverting the continued fraction form (eq. 1).

For the hydrostatic mapping function these coefficients b_h and c_h are taken from the hydrostatic part of the Isobaric Mapping Function IMF. If φ is the geodetic latitude, the coefficients are determined by $b_h = 0.002905$ and $c_h = 0.0634 + 0.0014 \cdot \cos(2\varphi)$ when φ is the latitude. For the wet part of VMF(fast), the coefficients b_w and c_w are constant for all

latitudes, because changes in a_w are sufficient to model the dependence of the wet mapping functions on latitude. They are taken from NMF ($\varphi = 45^\circ$: $b_w = 0.00146$ and $c_w = 0.04391$).

The procedure above shows that VMF(fast) is some kind of extension to smfw3 of IMF. The ratio of the wet path delay along a straight line at 3.3° elevation and its zenith delay (smfw3) is replaced by the 'quasi-true' mapping function value at 3.3° initial elevation angle. In contrast to IMFw (smfw3), the bending of the ray is taken into account, and the number of vertical steps is increased considerably for the computation (from 15 to about 1000) by interpolation in height between the pressure levels.

To check the quality of VMF(fast), the values of the mapping functions have been compared to VMF(rig) for CONT02. This is a continuous 15-days VLBI campaign with eight stations in October 2002. (More information about CONT02 is available at <http://ivscc.gsfc.nasa.gov/cont02>). For an elevation angle of 5° the RMS differences are about 5 mm for the hydrostatic and 1 mm for the wet part when the hydrostatic and wet zenith delays are assumed to be 2000 mm and 200 mm, respectively. This would imply that the corresponding error in the station height is about 2 mm when the cutoff elevation angle is set to 5° [Niell *et al.*, 2001]. Moreover, the RMS differences vanish at about 3° because VMF(fast) is tuned for this elevation angle, and above 5° elevation the RMS differences are also decreasing.

2.3 Mapping function parameters provided by IGG

The Institute of Geodesy and Geophysics (IGG) at the University of Technology, Vienna, gets regular access to data from the ECMWF (European Centre for Medium-Range Weather Forecasts). Derived parameters which are necessary to determine IMF and VMF for non-commercial purposes have been provided to the scientific community since September 2003. Table 1 gives an overview of the ECMWF datasets which are used for these computations. The parameters for IMF (z200 and smfw3) are provided on a global grid with a resolution of $2.5^\circ \times 2.0^\circ$. The coefficients a_h , a_w for the hydrostatic and wet part of VMF(fast) are determined for all geodetic VLBI stations. This list will be extended to other selected sites, e.g. the IGS (International GPS Service) stations. All parameters are given every six hours and they can be found at the webpage <http://www.hg.tuwien.ac.at/~ecmwf>.

Table 1. Specifications of the ECMWF datasets which are used for the computation of IMF and VMF.

	IMF	VMF
doy 1 in 1979 - doy 365 in 2001	2.5° x 2.0° ERA-40 Re-Analysis pressure level dataset (15 levels from 1000 to 10 hPa)	2.5° x 2.0° ERA-40 Re-Analysis pressure level dataset (15 levels from 1000 to 10 hPa)
doy 1 in 2002 - doy 238 in 2003	2.5° x 2.0° operational pressure level dataset (15 levels from 1000 to 10 hPa)	2.5° x 2.0° operational pressure level dataset (15 levels from 1000 to 10 hPa)
doy 239 in 2003 - now		operational pressure level dataset (21 levels from 1000 to 1 hPa, resolution 0.28125°)

3 Validation of the VMF

Improved mapping functions are expected to improve geodetic accuracies. Good measures for the quality of geodetic results are the 'baseline length repeatability' and the difference in baseline length when changing the cutoff elevation angle ('elevation angle cutoff test'). For the geodetic VLBI analysis, the classical least-squares method (Gauss-Markov model) of the OCCAM 5.1 VLBI software package [Titov *et al.*, 2001] is used. Free network solutions with a minimum of squared station coordinate residuals [Koch, 1999] are calculated for the 24 h sessions with five Earth orientation parameters being estimated (nutation, dUT1 and pole coordinates). Atmospheric loading parameters are obtained from Petrov and Boy [2003], ocean loading parameters from Scherneck and Bos [2002] using the CSR4.0 model by Eanes [1994], and total gradient offsets are estimated every 6 hours using the model by Davis *et al.* [1993]. An overview of the input parameters for NMF, IMF and VMF is given in table 2.

Table 2. Input parameters for hydrostatic and wet mapping functions of NMF, IMF, and VMF(fast). φ is the station latitude, h is the station height, and doym is the day of the year.

	NMF	IMF	VMF
hydrostatic	doy, h , φ	z200, φ , h	h , a (b , c from IMF)
wet	φ	smfw3, h	a (b , c from NMF)

3.1 Baseline length repeatabilities

Baseline length repeatabilities are determined for CONT02 (2002, October 16-31), and for all IVS-R1 and IVS-R4 sessions through August, 2003. IVS-R1 and IVS-R4 are weekly 24 h sessions observed on Mondays and Thursdays, respectively, starting in January 2002 [Nothnagel and Steinforth, 2003]. For the following investigations all baselines which include the station Tigo Concepcion (Chile) are excluded, because due to the small antenna dish (6 m diameter), the low SNR does not allow a reliable validation of the tropospheric mapping functions. Also, the baselines with station Gilmore Creek (Alaska, U.S.A.) are not considered before the Earthquake on November 3, 2002. The cutoff elevation angle was set to 5°.

Table 3 and table 4 provide information about the improvement of the baseline length repeatabilities of the CONT02, IVS-R1 and IVS-R4 sessions with VMF(fast) and IMF compared to NMF. Table 3 gives the percentage of improved baselines, and table 4 provides the mean value of the improvement over all baselines (eq. 2).

$$(2) \quad \delta = \frac{\sum_{i=1}^N \frac{(\sigma_{\text{NMF},i} - \sigma_{\text{VMV},i})}{\sigma_{\text{NMF},i}}}{N} \cdot 100$$

δ mean improvement over all baselines ($i = 1, \dots, N$)

σ repeatability (RMS of the baseline lengths w.r.t. a linear trend)

Table 3. Fraction of baselines with repeatabilities better than with NMF (in %). A clear majority of the baselines is improved with the mapping functions based on NWM.

	CONT02	IVS-R1	IVS-R4
IMF	54 %	79 %	80 %
VMF(fast)	70 %	78 %	74 %

Table 4. Mean values of the improvements in % (δ). The improvement is largest for the IVS-R1 sessions and the VMF(fast) (~ 11 %).

	CONT02	IVS-R1	IVS-R4
IMF	1.9 %	9.5 %	4.5 %
VMF(fast)	5.6 %	11.2 %	4.4 %

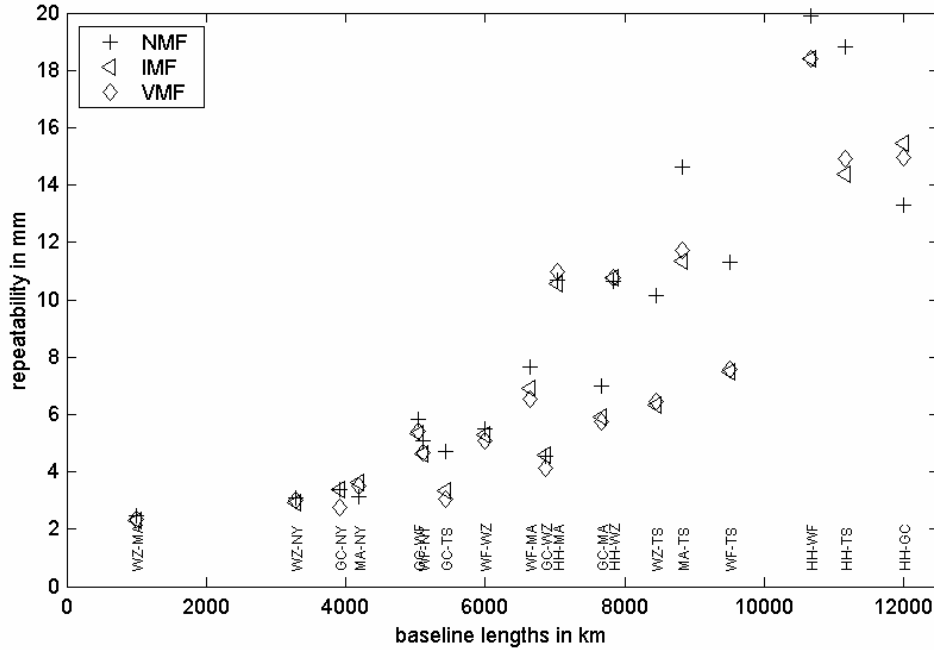


Figure 2. Baseline lengths repeatabilities for IVS-R1. For almost all baselines a clear improvement can be seen with the new mapping functions IMF and VMF. For the specification of the baselines the IVS 2-letter codes are used (see <http://ivscc.gsfc.nasa.gov/org/ns.html>). The longest baseline from Hartebeesthoek (South Africa) to Gilmore Creek (Alaska, U.S.A.) shows a clear degradation with IMF and VMF, possible reasons are mentioned in the text.

Figure 2 shows that nearly 80% of the IVS-R1 baseline lengths repeatabilities are improved with IMF and VMF(fast) compared to NMF. Only the longest baseline of about 12000 km from Hartebeesthoek (South Africa) to Gilmore Creek (Alaska, U.S.A.) has a clear degradation in repeatability. Either, this is due to bad numerical weather models at the two sites, or this is simply due to the bad geometry, because only few observations contribute to the determination of the baseline. Thereto, further investigations need to be done. Figure 3 shows a histogram for the improvements of the IVS-R1 baselines. It reveals that the clear majority of the baselines (15) is improved and the repeatabilities of four baselines only are degraded with IMF and VMF(fast) with respect to NMF.

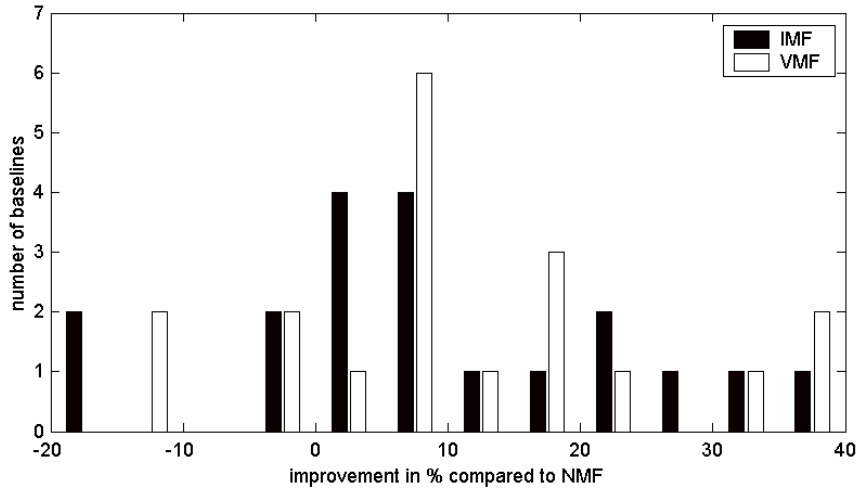


Figure 3. Histogram for the improvements in % of the IVS-R1 baselines with IMF and VMF(fast) compared to NMF. The baseline length repeatability is worse for four baselines only, whereas a clear majority of baselines is improved with the new mapping functions.

3.2 Elevation angle cutoff tests

Another measure for the quality of mapping functions can be obtained by elevation angle cutoff tests [Herring, 1983]. These tests show how baseline lengths change when the cutoff elevation angle is varied. They are a good measure for the absolute accuracy of the mapping functions, because if there is a systematic error in the mapping functions the baseline lengths will be influenced when the cutoff angle is changed. In figure 4, the differences in baseline lengths are shown for the IVS-R1 sessions when changing the cutoff elevation angle from 5° to 10° .

Figure 4 shows that almost all differences for NMF are above those for IMF and VMF(fast). This implies that the baseline lengths with a cutoff elevation angle of 5° are systematically longer with IMF and VMF(fast) than with NMF, since the baseline lengths hardly differ when the cutoff elevation angle is set to 10° . This might be due to systematic effects in either of the mapping functions, and further investigations have to be performed to reveal the actual error sources.

Table 5 summarizes the elevation angle cutoff tests for CONT02, IVS-R1 and IVS-R4. It shows the RMS differences over all baselines when changing the cutoff elevation angle from 10° to 5° . Although modern mapping functions like IMF and VMF have their strengths especially at low elevations, there are no clear improvements or degradations with IMF and VMF, which is a confirmation that the quality of NMF is already rather good.

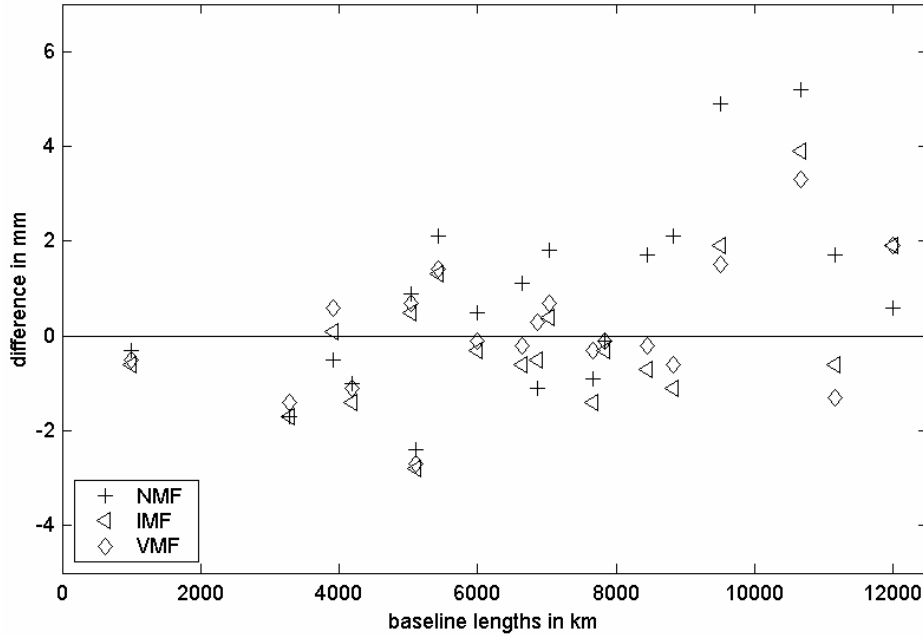


Figure 4. Elevation angle cutoff test for IVS-R1 (10° minus 5°). It can be seen that nearly all differences from NMF are above those from IMF and VMF(fast).

Table 5. RMS differences over all baselines when changing the cutoff elevation angle from 10° to 5° (in mm; smaller is better).

	CONT02	IVS-R1	IVS-R4
NMF	3.0	2.1	3.7
IMF	2.6	1.5	3.7
VMF(fast)	3.1	1.3	4.2

4 Conclusions and outlook

Recent mapping functions such as IMF and VMF based on data from numerical weather models like ECMWF provide better repeatabilities of baseline lengths. There is a mean improvement of 5% to 10% versus results obtained by NMF, but still, further investigations remain to be done. Especially, the quality of the mapping functions at certain stations has to be evaluated by means of nearby radiosonde data or different numerical weather models, and a closer look needs to be taken at the systematic effects in the elevation angle cutoff tests.

So far, baseline length repeatabilities are not significantly better with VMF compared to IMF, although VMF exploits the NWM more rigorously. But as the time series get longer, one might speculate that the advantages of VMF become visible, since starting with day 239 in 2003 the vertical and horizontal resolution of the ECMWF data has increased significantly (to

21 levels and down to 0.5° , respectively), and the quality of ECMWF data will improve steadily in the future.

Acknowledgements

We acknowledge the Zentralanstalt für Meteorologie und Geodynamik (ZAMG), Vienna, for providing regular access to the ECMWF data. We are also grateful to A.E. Niell for very informative discussions about NWM and mapping functions.

References

Boehm, J., and H. Schuh, Vienna Mapping Functions, *Proceedings of the 16th Working Meeting on European VLBI for Geodesy and Astrometry*, Leipzig, May 9-10, 2003, Verlag des Bundesamtes für Kartographie und Geodäsie, 131-143, 2003.

Davis, J.L., T.A. Herring, I.I. Shapiro, A.E.E. Rogers and G. Elgered, Geodesy by Radio Interferometry: Effects of Atmospheric Modeling Errors on Estimates of Baseline Length, *Radio Science*, Vol. 20, No. 6, 1593-1607, 1985.

Davis, J.L., G. Elgered, A.E. Niell, C.E. Kuehn, Ground-based measurement of gradients in the "wet" radio refractivity of air, *Radio Science*, Vol. 28, No. 6, 1003-1018, 1993.

Eanes, R.J., Diurnal and semidiurnal tides from TOPEX/POSEIDON altimetry. *Eos Trans. AGU*, 75(16):108, 1994.

Herring, T.A., Precision and accuracy of intercontinental distance determinations using radio interferometry, *Ph.D. Thesis*, Massachusetts Institute of Technology, Cambridge, Massachusetts, 1983. Also published as Air Force Geophysics Laboratory report AFGL-TR-84-0182.

Herring, T.A., Modelling atmospheric delays in the analysis of space geodetic data, *Symposium on Refraction of Transatmospheric Signals in Geodesy*, Netherlands Geod. Commis. Ser. 36, edited by J.C. DeMunk and T.A. Spoelstra, pp. 157-164, Ned. Comm. voor Geod., Delft, 1992.

Koch, K.R., Parameter Estimation and Hypothesis Testing in Linear Models, *Springer, Berlin*, 1999.

Marini, J.W., Correction of satellite tracking data for an arbitrary tropospheric profile, *Radio Science*, Vol. 7, No. 2, 223-231, 1972.

Niell, A.E., Global mapping functions for the atmosphere delay at radio wavelengths, *JGR, Vol. 101*, No. B2, 3227-3246, 1996.

Niell, A.E., Preliminary evaluation of atmospheric mapping functions based on numerical weather models, *Phys. Chem. Earth*, 26, 475-480, 2001.

Niell, A.E., A.J. Coster, F.S. Solheim, V.B. Mendes, P.C. Toor, R.B. Langley, and C.A. Upham, Comparison of Measurements of Atmospheric Wet Delay by Radiosonde, Water Vapor Radiometer, GPS and VLBI, *Journal of Atmospheric and Oceanic Technology*, 18, 830-850, 2001.

Nothnagel, A., and C. Steinforth, Analysis Coordinator Report, *International VLBI Service for Geodesy and Astrometry 2002 Annual Report*, edited by N. R. Vandenberg and K. D. Baver, NASA/TP-2003-211619, 68-69, 2003.

Petrov, L., and J.P. Boy, Study of the atmospheric pressure loading signal in VLBI observations, *submitted to JGR*, 2003.

Scherneck, H.-G., and M.S. Bos, Ocean Tide and Atmospheric Loading, *International VLBI Service for Geodesy and Astrometry 2002 General Meeting Proceedings*, edited by Nancy R. Vandenberg and Karen D. Baver, NASA/CP-2002-210002, 205-214, 2002.

Titov, O., V. Tesmer, and J. Boehm, Occam Version 5.0 Software User Guide, *Auslig Technical Report 7*, 2001.

Johannes Böhm, Birgit Werl, and Harald Schuh

Troposphere mapping functions for GPS and VLBI
from ECMWF operational analysis data

Journal of Geophysical Research

Vol. 111, B02406, doi:10.1029/2005JB003629

2006a

Troposphere mapping functions for GPS and VLBI from ECMWF operational analysis data

Johannes Böhm, Birgit Werl, and Harald Schuh

Abstract

In the analyses of geodetic VLBI and GPS data the analytic form used for mapping of the atmosphere delay from zenith to the line-of-site is most often a three parameter continued fraction in $1/\sin(\text{elevation})$. Using the 40 years reanalysis (ERA-40) data of the ECMWF (European Centre for Medium-Range Weather Forecasts) for the year 2001, the b and c coefficients of the continued fraction form for the hydrostatic mapping functions have been re-determined. Unlike previous mapping functions based on data from numerical weather models (Isobaric Mapping Functions IMF [Niell, 2000], Vienna Mapping Functions VMF [Boehm and Schuh, 2004]), the new c coefficients are dependent on the day of the year, and unlike the Niell Mapping Functions NMF [Niell, 1996] they are no longer symmetric with respect to the equator (apart from the opposite phase for the two hemispheres). Compared to VMF, this causes an effect on the VLBI or GPS station heights which is constant and as large as 2 mm at the equator and which varies seasonally between 4 mm and 0 mm at the poles. The updated VMF, based on these new coefficients and called VMF1 hereafter, yields slightly better baseline length repeatabilities for VLBI data. The hydrostatic and wet mapping functions are applied in various combinations with different kinds of a priori zenith delays in the analyses of all VLBI IVS-R1 and IVS-R4 24-hour sessions of 2002 and 2003; the investigations concentrate on baseline length repeatabilities, as well as on absolute changes of station heights.

1 Introduction

Modeling the path delays due to the neutral atmosphere for microwave signals emitted by satellites or radio sources is one of the major error sources in the analyses of Global Positioning System (GPS) and Very Long Baseline Interferometry (VLBI) observations. The concept is based on the separation of the path delays, ΔL , into a hydrostatic and a wet part [e.g., Davis *et al.*, 1985].

$$(1) \quad \Delta L(e) = \Delta L_h^z \cdot mf_h(e) + \Delta L_w^z \cdot mf_w(e)$$

In equation 1, the total delays $\Delta L(e)$ at an elevation angle e are made up of a hydrostatic (index h) and a wet (index w) part, and each of these terms is the product of the zenith delay (ΔL_h^z or ΔL_w^z) and the corresponding mapping function mf_h or mf_w . These mapping functions, which are independent of the azimuth of the observation, have been determined for the hydrostatic and the wet part separately by fitting the coefficients a , b , and c of a continued fraction form [Marini, 1972] (equation 2) to standard atmospheres [e.g., Chao, 1974], to radiosonde data [Niell, 1996], or recently to numerical weather models (NWMs) [e.g., Niell, 2000; Boehm and Schuh, 2004].

$$(2) \quad mf(e) = \frac{1 + \frac{a}{1 + \frac{b}{1 + c}}}{\sin e + \frac{a}{\sin e + \frac{b}{\sin e + c}}}$$

Whereas the hydrostatic zenith delays, ΔL_h^z (m), which can be determined from the total pressure p in hPa and the station coordinates (latitude ϕ and height h in m) at a site [Saastamoinen, 1973] (equation 3), and the hydrostatic and wet mapping functions are assumed to be known, the wet zenith delays, ΔL_w^z , are estimated within the least-squares adjustment of the GPS or VLBI analyses.

$$(3) \quad \Delta L_h^z = 0.0022768 \cdot \frac{p}{(1 - 0.00266 \cdot \cos(2\phi) - 0.28 \cdot 10^{-6} \cdot h)}$$

However, there might be errors in the hydrostatic zenith delays or the mapping functions, and their influence on station heights is well described with a rule of thumb by Niell *et al.* [2001]: *The error in the station height is approximately one third of the delay error at the lowest elevation angle included in the analysis.* Following a refinement of this rule of thumb by Boehm [2004], the factor is rather 1/5 than 1/3 for a minimum elevation angle of 5° , which is also close to the value 0.22 found by MacMillan and Ma [1994]. The following two examples illustrate this rule of thumb, which holds for both GPS and VLBI, but which depends on the actual distribution of elevations and on whether elevation-dependent weighting is used: The

hydrostatic and wet zenith delays are taken to be 2000 mm and 200 mm, respectively, the minimum elevation angle is 5° , and the corresponding values for the hydrostatic and wet mapping functions are 10.15 ($mf_h(5^\circ)$) and 10.75 ($mf_w(5^\circ)$). (1) We assume an error in the total pressure measured at the station of 10 hPa: 10 hPa correspond to ~ 20 mm hydrostatic zenith delay (compare equation 3), which is then mapped down with the wrong mapping function (factor $0.6 = 10.75 - 10.15$). At 5° elevation the mapping function error is 12 mm, and one fifth of it, i.e. 2.4 mm, would be the resulting station height error. (2) We consider an error in the wet mapping function of 0.01 ($mf_w(5^\circ) = 10.76$ instead of 10.75) or in the hydrostatic mapping function of 0.001 ($mf_h(5^\circ) = 10.151$ instead of 10.15). The error at 5° elevation in both cases is 20 mm, i.e. the error in the station height would be approximately 4 mm.

The Vienna Mapping Functions (VMF) introduced by *Boehm and Schuh* [2004] depend only on elevation angle and not on azimuth, i.e. they assume that the troposphere is symmetric around the stations. For the b and c coefficients (see equation 2) the best values available at that time were taken from the Isobaric Mapping Functions (IMF) [*Niell and Petrov*, 2003] for the hydrostatic part and from the Niell Mapping Functions (NMF) at 45° latitude [*Niell*, 1996] for the wet part. Figure 8 shows the hydrostatic mapping function from NMF and VMF for the station Algonquin Park in 2002 and 2003. In section 2, an updated version for the VMF [*Boehm and Schuh*, 2004] is developed, which is based on new b and c coefficients for the hydrostatic mapping functions and which will be called VMF1 hereafter. For VMF1, the c coefficients from raytracing are fit to a function of latitude and day of year to remove systematic errors. This is important for geophysical applications of geodesy, for instance, to determine the correct seasonal and latitude dependence of hydrology. An alternative approach to the traditional separation into wet and hydrostatic mapping functions is the introduction of the ‘Total’ Vienna Mapping Function’ (VMF1-T) for mapping down the total delays, which uses the total refractivity instead of its hydrostatic and wet components. In section 3 different procedures are described for calculating a priori zenith delays that can be used for GPS and VLBI analyses, including their determination from the operational analysis pressure level dataset of the ECMWF (European Centre for Medium-Range Weather Forecasts). In section 4, the impact of the different mapping functions and of the different a priori zenith delays on geodetic results is investigated using all IVS-R1 and IVS-R4 24-hour sessions of 2002 and 2003, including CONT02. CONT02 was a two-week continuous VLBI campaign in the second half of October 2002 [*Thomas and MacMillan*, 2003].

2 New hydrostatic b and c coefficients for VMF1

At the ECMWF, the ERA-40 (ECMWF Re-Analysis 40-years) data are stored as expansions of spherical harmonics with a horizontal resolution corresponding to about 125 km [Simmons and Gibson, 2000]. From these data, monthly mean profiles for the year 2001 (for the epochs 0, 6, 12, and 18 UT) were downloaded on a global grid (30° in longitude by 15° in latitude). These profiles consist of 23 levels from 1000 hPa to 1 hPa (1000, 925, 850, 775, 700, 600, 500, 400, 300, 250, 200, 150, 100, 70, 50, 30, 20, 10, 7, 5, 3, 2, 1), and they comprise values for height, total pressure, temperature, and water vapor pressure for each level.

2.1 Determination of the b and c coefficients

In a first step, for all 7488 profiles (156 grid points times 12 months times 4 epochs per day) the total and hydrostatic mapping functions as well as the vacuum elevation angles e are determined for 10 different initial elevation angles e_0 (3.2°, 5°, 7°, 10°, 15°, 20°, 30°, 50°, 70°, 90°) [compare Boehm, 2004]. The vacuum elevation is the asymptotic final elevation angle of the outgoing ray and corresponds to the direction expected for the target observed, either the GPS satellite or the VLBI radio source. The geometric bending effect ΔL_{bend} [see Davies *et al.*, 1985] is added to the hydrostatic and to the total mapping functions (equations 4 and 5).

$$(4) \quad \text{mf}_h(e) = \frac{\Delta L_h(e) + \Delta L_{\text{bend}}(e)}{\Delta L_h^z}$$

$$(5) \quad \text{mf}_t(e) = \frac{\Delta L_h(e) + \Delta L_w(e) + \Delta L_{\text{bend}}(e)}{\Delta L_h^z + \Delta L_w^z}$$

Then, the three coefficients a , b , and c of the total and hydrostatic mapping functions (equation 2) are fitted to the ten discrete mapping function values of each profile by a least-squares adjustment. The residuals of their fit are usually smaller than 0.5 mm. These 7488 mapping functions will be used as 'rigorous' reference for evaluations in section 2.2. The mean value of all b coefficients for both the total (index t) and hydrostatic (index h) mapping functions is found to be

$$(6) \quad b_t = b_h = 0.0029,$$

and is kept fixed in all further analyses. In the next step the least-squares adjustment is repeated, but only the coefficients a and c are estimated for all profiles, while the coefficient b for the hydrostatic and total mapping functions is kept fixed to the value given in equation 6. The coefficients c then show a clear variability depending on season and latitude, but unlike former mapping functions, the coefficients c are not symmetric with respect to the equator (apart from the phase offset for the two hemispheres). For example, the coefficient c at the North pole in January is significantly smaller than c at the South pole in July (figure 1).

Therefore, equation 7 is used to model the coefficient c , when doy is the day of the year and 28 January has been adopted as the reference epoch [Niell, 1996], φ is the latitude, and ψ specifies the northern or southern hemisphere (see the last columns of table 1 and 2).

$$(7) \quad c = c_0 + \left[\left(\cos \left(\frac{\text{doy} - 28}{365} \cdot 2\pi + \psi \right) + 1 \right) \cdot \frac{c_{11}}{2} + c_{10} \right] \cdot (1 - \cos \varphi)$$

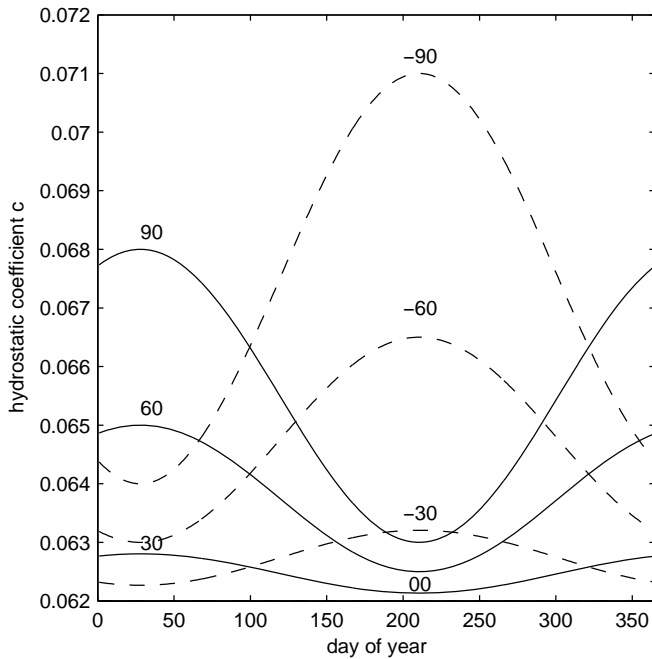


Figure 1. Hydrostatic coefficients c for 0° , $\pm 30^\circ$, $\pm 60^\circ$, and $\pm 90^\circ$ latitude in 2001 from ERA-40 data (equation 7).

Table 1 and table 2 contain the parameters of equation 7 which are obtained for the hydrostatic and total mapping functions. As an example, the coefficient c in January 2001 is plotted in figure 1 for different latitudes.

Table 1. Parameters c_0 , c_{10} , c_{11} , and ψ needed for computing the coefficient c (eq. 7) of the hydrostatic mapping function (eq. 4).

hemisphere	c_0	c_{10}	c_{11}	ψ
northern	0.062	0.001	0.005	0
southern	0.062	0.002	0.007	π

Table 2. Parameters c_0 , c_{10} , c_{11} , and ψ needed for computing the coefficient c (eq. 7) of the total mapping function (eq. 5).

hemisphere	c_0	c_{10}	c_{11}	ψ
northern	0.063	0.000	0.004	0
southern	0.063	0.001	0.006	π

The b and c coefficients of the wet mapping functions do not have to be changed because the wet zenith delays are smaller by a factor of ~ 10 than the hydrostatic zenith delays and the effect of variations in b and c is not significant. The b and c coefficients of the wet mapping function are still fixed to those of NMF [Niell, 1996] at 45° latitude and the coefficient a is estimated for each profile, i.e., the recommended wet mapping function is still VMF(wet).

2.2 Evaluation of the new coefficients

The 'fast' approach (in which the parameter a is estimated from a single raytrace at initial elevation angle $e_0 = 3.3^\circ$) can be compared with the 'rigorous' approach that determines all three coefficients in a least-squares adjustment using ten different initial elevation angles. The maximum differences are encountered at 5° elevation because the 'fast' mapping functions (VMF1) are 'tuned' for elevations of $\sim 3^\circ$, i.e. there is no error at $\sim 3^\circ$, while at elevation angles considerably higher than 5° the differences between the rigorous and the fast approach are also vanishing. With the new b and c coefficients (equation 7 and tables 1 and 2), the deviation from the rigorous approach at 5° elevation is always smaller than 8 mm, which means that the corresponding error in the station height is always smaller than 1.6 mm. This holds for all months in 2001 and for all latitudes and longitudes (see table 3).

Table 3. Mean biases and standard deviations of hydrostatic delay differences at 5° elevation for NMF, VMF, and VMF1 with respect to the hydrostatic mapping functions derived from the numerical weather model for a global grid and 12 months in 2001. In parentheses the equivalent station height errors are given.

	mean bias [mm]	standard deviation [mm]
NMF	21.8 (4.4)	35.0 (7.0)
VMF	3.3 (0.7)	11.2 (2.2)
VMF1	2.3 (0.5)	2.0 (0.4)

The principle of VMF1 (which is the principle of VMF(fast) in [Boehm and Schuh, 2004]) is to use the best coefficients b and c available, determine the values of the mapping functions at $e_0 = 3.3^\circ$ initial elevation angle from the NWM, and derive the coefficient a by simply inverting the continued fraction form (equation 2). In our study, the values of the mapping functions for the VLBI and GPS stations are determined from the ECMWF operational pressure level data. No horizontal interpolation for the sites has to be done between grid points because the latitudes and longitudes of the stations are input parameters to the expansion of spherical harmonics of the operational pressure level data corresponding to a horizontal resolution of about 0.3° . With VMF1 no height correction is necessary (compare Niell [1996]), since the raytracing starts at the actual station height. To get the meteorological parameters at the position of each site, the temperature is interpolated linearly between the pressure levels, and the total and water vapor pressure are interpolated exponentially applying the hypsometric equation (see also [Boehm, 2004]). Figure 2 shows the differences of the hydrostatic delays at 5° elevation between VMF [Boehm and Schuh, 2004] and VMF1 (this paper) for 213 IGS (International GPS Service) stations for the day 28 in 2005 (January) and the day 210 in 2004 (July) (at 0, 6, 12, and 18 UT). It can be seen that the two hydrostatic mapping functions agree best at mid-latitudes, but that there are systematic differences closer to the equator and near the winter poles which are caused by deficiencies of the c coefficients in VMF [Boehm and Schuh, 2004]. These systematic errors of VMF were not detected by Boehm and Schuh [2004], since they made their checks only for the CONT02 stations which are situated mostly at mid-latitudes where the 'fast' VMF agrees well with the 'rigorous' approach. (For the investigations presented here, a global grid of profiles for the complete year 2001 has been used to validate VMF1.)

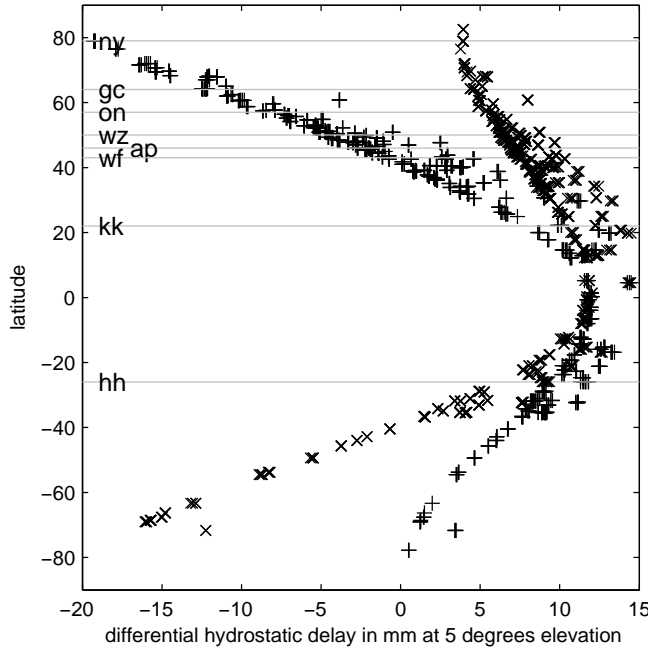


Figure 2. Hydrostatic delay differences (in mm) VMF minus VMF1 on day of year 28 in 2005 (+) and on day of year 210 in 2004 (x) at 5° elevation for 213 IGS stations. Additionally, the latitudes of the eight CONT02 stations are marked by thin horizontal lines. A differential hydrostatic delay of -20 mm at the North pole corresponds to an apparent station height change of about -4 mm when using VMF1 instead of VMF.

For the VMF [Boehm and Schuh, 2004], the hydrostatic b and c coefficients were taken from the Isobaric Mapping Functions IMF [Niell and Petrov, 2003], but it has to be mentioned that the development of IMF was based on radiosonde data which were taken mainly at mid-latitudes where the agreement between VMF and VMF1 is very good. In our work here, a global distribution was used to derive functions for the b and c coefficients, and this allowed detection of deficiencies at the winter poles and near the equator of earlier hydrostatic mapping functions.

Table 3 shows the mean biases and standard deviations of the hydrostatic delays at 5° elevation (assuming 2000 mm hydrostatic zenith delay) between reference values determined from raytracing through the numerical weather model at all grid points described at the beginning of section 2.1 and those from NMF, VMF, and VMF1, respectively. The minor standard deviation of 2 mm between the raytraced mapping function at 5° elevation and VMF1 justifies the exclusive determination of the coefficient a instead of all three coefficients a, b, and c. Contrarily, there are significant delay errors with NMF which are equivalent to station height errors of 4 mm (bias) and 7 mm (standard deviation), respectively. Niell [2005, personal communication], has compared VMF1 with mapping functions derived from

radiosonde data, and he found equivalent station height errors of less than 2 mm, which is similar to the values reported by *MacMillan and Ma* [1998] for differences between mapping functions from radiosonde data and numerical weather models at four selected sites.

2.3 Vienna Total Mapping Function (VMF1-T)

Instead of separating the delays into a hydrostatic and a wet part, an alternative concept of total delays has also been investigated for tropospheric modeling, that is the use of a single total mapping function mf_t (equation 5) for mapping down the a priori total zenith delays $\Delta L_{t,0}^z$ and as partial derivative for the estimation of the residual total delays $\Delta L_{t,res}^z$ (equations 8 and 9).

$$(8) \quad \Delta L_t^z = \Delta L_h^z + \Delta L_w^z = \Delta L_{t,0}^z + \Delta L_{t,res}^z$$

$$(9) \quad \Delta L(e) = \Delta L_{t,0}^z \cdot mf_t(e) + \Delta L_{t,res}^z \cdot mf_t(e)$$

A benefit of the numerical weather models is that they enable the determination of not only the total mapping functions (equation 5) but also of the a priori total zenith delays. Although for the analysis of VLBI sessions in section 4 a priori total zenith delays are used, a priori hydrostatic zenith delays could have been applied, too, because the mapping function for the a priori zenith delays is the same as for the residual zenith delays.

With the classical separation into a hydrostatic and a wet part, errors of the hydrostatic zenith delays cannot be fully compensated for by estimating the remaining wet part, because the hydrostatic and wet mapping functions are significantly different, especially at low elevations. The advantage of this concept is that it cannot be affected by poor a priori hydrostatic zenith delays. On the other hand, the total mapping function is close in value to the hydrostatic mapping function, which allows estimation of the residual hydrostatic delays properly only if a) the wet zenith delays have been accurately calculated from the ECMWF, and b) they do not differ from the linear interpolation between 6-hour values that is used to construct the a priori total delay.

A limitation to the concept of the total mapping function is that it is affected by bad a priori information about the wet part in the atmosphere from the numerical weather models. *Snajdrova et al.* [2005] show that the wet zenith delays determined from pressure level data of the ECMWF and the wet zenith delays estimated in the VLBI analysis for CONT02 agree at

the 1 cm level in terms of bias and up to the 2 cm level (for stations with high humidity like Kokee Park) in terms of scatter (compare table 4). While a bias of 1 cm is not that critical (corresponds to a bias of 1.2 mm in station height), a noise of about 3 mm is added to the vertical scatter at humid sites. But even if the information about the hydrostatic and wet part provided by the numerical weather models at the 6-hour time epochs was accurate at the mm level, the total mapping function would not be able to perfectly model the path delays since the variation - especially in the wet part - is more rapid than can be modeled with 6-hour time intervals (figure 3). This again adds noise to the station heights and baseline lengths (see figure 6), because the total mapping function, which is close to the hydrostatic mapping function, is not appropriate to estimate these rapid variations of the wet zenith delays.

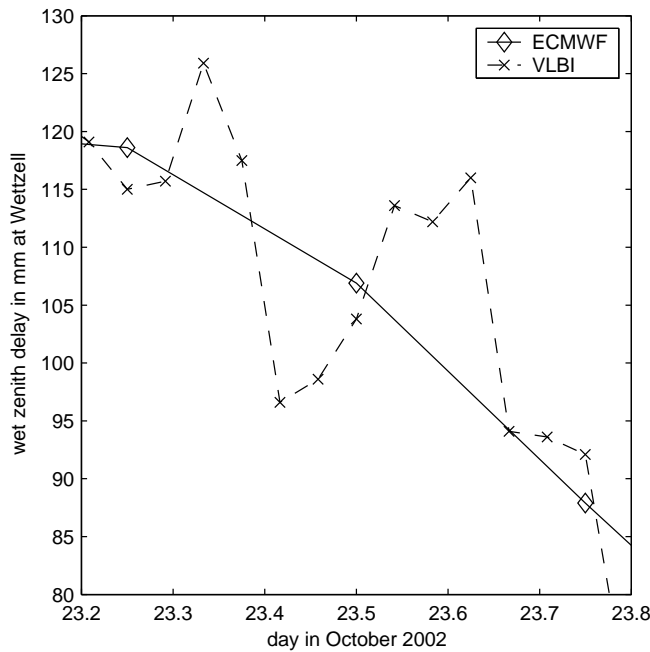


Figure 3. Wet zenith delays in mm at station Wettzell on 23 October 2002. It shows that there is more variation in the wet zenith delays than can be modeled with 6-hour data from the ECMWF.

3 A priori zenith delays

Three different methods are compared for obtaining the a priori hydrostatic zenith delays. They are determined from either of the two sources of station pressure values, or from numerical integration through pressure level data of the ECMWF. In the case of pressure values, these are taken either from the pressure sensors at the stations or from a standard model which yields the pressure for a given height h according to [Berg, 1948] (equation 10):

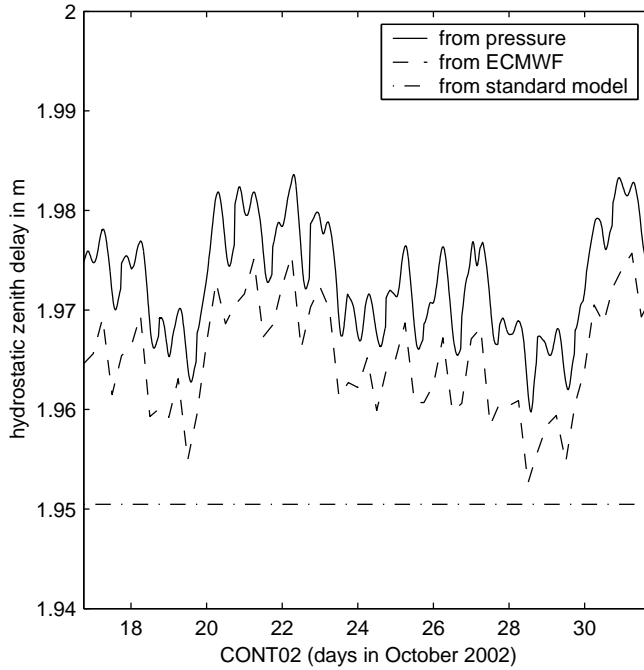


Figure 4. A priori hydrostatic zenith delays at Hartebeesthoek (South Africa) determined (1) from the pressure values at the site, (2) from ECMWF data, and (3) from a standard model for the pressure (equation 10).

$$(10) \quad p = 1013.25 \cdot (1 - 0.0000226 \cdot h)^{5.225}$$

The hydrostatic delay is then calculated using *Saastamoinen* [1973] (equation 3). Figure 4 shows the different hydrostatic zenith delays at Hartebeesthoek (South Africa) during CONT02. While the hydrostatic zenith delays derived from pressure readings at the site and those from the numerical weather model are similar (apart from a bias), the hydrostatic zenith delays from the standard model are constant with time. Table 4 summarizes the biases and standard deviations between the hydrostatic zenith delays from the observed pressure values on the one hand and those from the numerical weather model ECMWF and the standard model for the pressure on the other hand at eight VLBI sites during the CONT02 campaign.

The hydrostatic zenith delays at station Wettzell in Germany as derived from the numerical weather model are in error by about 16 mm (compared to the observed pressure values), i.e. an error of 16 mm is mapped down with the wrong mapping function. If the cutoff elevation angle is set to 5° , the delay error at 5° is 10 mm ($= (10.75 - 10.15) \cdot 16$ mm, see section 1) and the corresponding station height error is about 2 mm (compare figure 7). Thus, the error is due to using the wet mapping function with the wrong a priori zenith hydrostatic delay. At the other stations the effect is smaller. With the concept of the total mapping functions, the error

in the a priori hydrostatic zenith delays is of less importance because errors in the a priori zenith delays are corrected by estimating the residual total zenith delays (equation 9) in the least-squares fit.

However, at Wettzell for example, the wet bias of 13 mm then introduces a height error (bias) of approximately 2 mm, so the total mapping function does not significantly reduce the error even though it allows correction for the hydrostatic error. The total mapping function will in addition cause even larger errors in the total delay because of the error in the wet delay between the times of NWM input, and because the standard deviation of the wet delay from the NWM is four times larger than that of the hydrostatic delay.

Table 4. Biases and standard deviations in mm of the hydrostatic zenith delays derived from ECMWF data and the standard model for the pressure with respect to the hydrostatic zenith delays determined from the observed pressure values at eight VLBI sites in the second half of October 2002 (CONT02). The last two columns show the biases and standard deviations of the wet zenith delays between estimates from VLBI analyses and ECMWF data [Snajdrova et al., 2005].

	hydr. zenith delays [mm] (observed pressure - ECMWF)		hydr. zenith delays [mm] (observed pressure - standard model)		wet zenith delays [mm] (VLBI estimates - ECMWF)	
	bias	std.dev.	bias	std.dev.	bias	std.dev.
Algonquin Park	5	1	-8	17	-12	3
Gilmore Creek	-5	2	11	16	-8	12
Hartebeesthoek	-8	1	-23	5	-5	20
Kokee Park	-7	1	22	3	-9	21
Ny-Ålesund	-8	2	13	26	+7	5
Wettzell	-16	2	-13	16	+13	9
Westford	6	1	-5	16	-16	6
Onsala	-14	2	12	23	+8	6

4 Validation in VLBI analyses

4.1 Analysis setup

Table 5. Mapping functions which are used in the VLBI analyses of the IVS-R1 and IVS-R4 sessions of 2002 and 2003 (and CONT02). There are variations of the NMF [Niell, 1996], the VMF [Boehm and Schuh, 2004], and the VMF1 (this paper) used in combinations with different kinds of a priori zenith delays. The lowercase indices h and w refer to 'hydrostatic' and 'wet' mapping functions.

abbrev.	a priori zenith delay		mapping of a priori zenith delay	partial derivative
	refractivity	type		
NMF	hydrostatic	pressure	NMFh	NMFw
NMF-X	hydrostatic	std. model	NMFh	NMFw
NMF-Y	total	ECMWF	NMFh	NMFh
VMF	hydrostatic	pressure	VMFh	VMFw
VMF1	hydrostatic	pressure	VMF1h	VMFw
VMF1-X	hydrostatic	ECMWF	VMF1h	VMFw
VMF1-T	total	ECMWF	VMF1-T	VMF1-T

Table 5 summarizes the mapping functions and a priori zenith delays that have been used for the analyses of all IVS-R1 and IVS-R4 sessions of 2002 and 2003 (including CONT02). NMF is the classical mapping function provided by *Niell* [1996] with the a priori hydrostatic zenith delays determined from pressure values recorded at the sites. In addition to that, two modifications of NMF are used for comparisons: NMF-X with a priori hydrostatic zenith delays determined from the standard pressure model [*Berg*, 1948], and NMF-Y with the hydrostatic NMF (NMFh) as total mapping function, i.e. NMFh is applied to map down the a priori total zenith delays from ECMWF, and as partial derivative to estimate the residual zenith delays. Both the NMF-X and NMF-Y comparisons are of interest because it is possible to select these options in some GPS software packages [*Hugentobler et al.*, 2001]. In addition to the VMF published by *Boehm and Schuh* [2004], various versions of VMF1 (this paper) are compared: VMF1 applies a priori hydrostatic zenith delays from observed pressure values at the sites, VMF1-X uses a priori hydrostatic zenith delays from ECMWF, and VMF1-T is the VMF1 for the total zenith delays as described in section 2.3.

For the geodetic VLBI analyses, the classical least-squares method (Gauss-Markov model) of the OCCAM 6.0 VLBI software package [Titov *et al.*, 2001] is used. Free network solutions with no-net translation and no-net rotation conditions [Koch, 1999] are calculated for the 24-hour sessions with five Earth orientation parameters being estimated (nutation, dUT1, and pole coordinates). Atmospheric loading parameters are obtained from Petrov and Boy [2003], and ocean loading corrections are calculated from Scherneck and Bos [2002] using the CSR4.0 ocean tide model by Eanes [1994]. The zenith delays are estimated as 1-hour continuous piecewise linear functions, and total gradients are estimated as 6-hour offsets using the model by Davis *et al.* [1993]. The cutoff elevation angle is set to 5° for all sessions.

4.2 Baseline length repeatabilities

For each baseline, the repeatability σ can be determined as the standard deviation of the n estimates b_i with regard to the mean value b_0 on a regression polynomial of first order (equation 11).

$$(11) \quad \sigma = \sqrt{\frac{\sum_{i=1}^n (b_i - b_0)^2}{n - 2}}$$

The power of the improvement in mm^2 (reduction of variance) with a certain mapping function compared to NMF [Niell, 1996] is determined as the quadratic standard deviation σ_{NMF}^2 minus σ^2 from the tested mapping function. For the following investigations all IVS-R1 and IVS-R4 sessions in 2002 and 2003 as well as the CONT02 sessions were analyzed, but only those 40 baselines which are made up of the eight VLBI stations which took part in CONT02 (see table 4) plus the sites Matera in Italy and Tsukub32 in Japan are shown for the statistics below.

Figure 5 shows the reduction in variance of baseline length repeatability versus baseline length. There is a clear improvement with VMF and VMF1 compared to NMF, with the largest improvements for baselines with Tsukub32 (ts). This is due to the fact that the sites in Japan do not fit into the climatological model that is inherent to NMF. Three baselines from Hartebeesthoek (South Africa) (to Kokee Park (kk), Algonquin Park (ap), and Matera (ma)) are significantly worse with both VMF and VMF1 compared to NMF. At Hartebeesthoek, it has repeatedly been seen that the results with mapping functions based on information from

the ECMWF do not surpass NMF [Boehm and Schuh, 2004], which might be due to rather poor ECMWF data in this region. Comparing the variances from VMF1 with those from VMF in figure 5, it is evident that VMF1 yields a slightly better precision for most of the baselines (33 out of 40).

Figure 6 shows the median reduction of variance (over all 40 baselines) in mm^2 compared to the repeatabilities from NMF. A clear improvement can be seen for VMF [Boehm and Schuh, 2004], and especially for all variations of VMF1. This demonstrates that there is a small improvement with the concept of the new b and c coefficients of VMF1 described in this paper, even if the stations are not situated near the equator and at the poles where the deficiencies of VMF are most critical. VMF1 is slightly degraded by introducing a priori hydrostatic zenith delays from ECMWF (VMF1-X) and even more by using the concept of the total mapping function (VMF1-T), as explained in section 2.3. NMF gives better precision over NMF-X and NMF-Y since the measured pressure (using equation 3) must give the best hydrostatic zenith delay and NMF-Y is substantially mismodeling the elevation dependence of the wet delay.

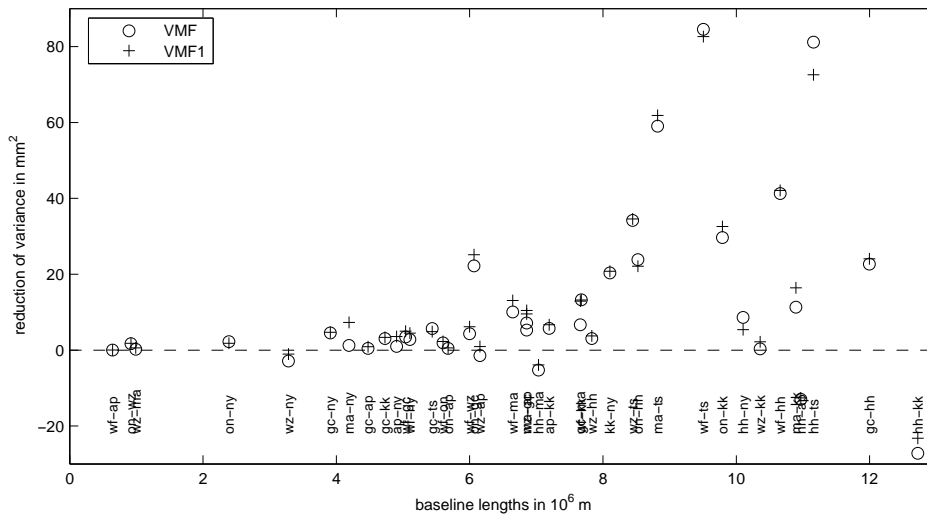


Figure 5. Variance reduction versus baseline length for all VLBI IVS-R1, IVS-R4, and CONT02 sessions in 2002 and 2003 (see text section 4.2 for baselines used). There is a clear improvement of both VMF and VMF1 compared to NMF. Only three baselines from Hartebeesthoek (to Kokee Park (kk), Algonquin Park (ap), and Matera (ma)) are significantly worse with both VMF and VMF1 compared to NMF. There is a huge improvement for baselines with the station Tsukub32 in Japan.

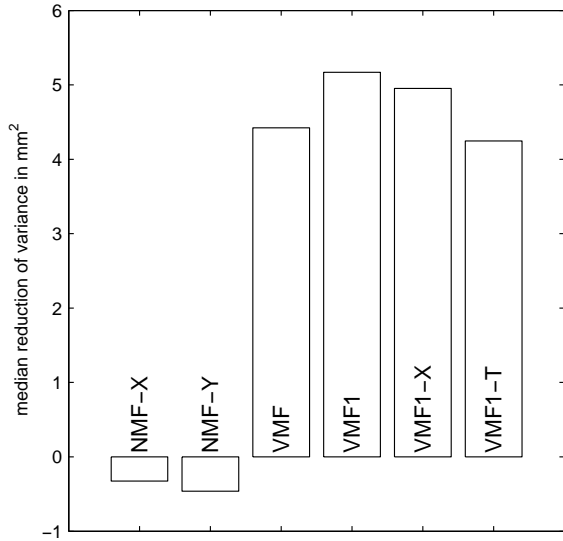


Figure 6. Median reduction of variance in mm^2 of the baseline length repeatabilities of all VLBI IVS-R1, IVS-R4, and CONT02 sessions in 2002 and 2003 with regard to NMF. A clear improvement is evident for VMF and all VMF1s. The best repeatability is achieved for VMF1 with the hydrostatic zenith delays determined from the observed pressure values.

4.3 Baseline lengths

The changes of the baseline lengths db can be converted into station height changes dh by using a least-squares adjustment with the Jacobian matrix based on the geometry of the baselines (equation 12).

$$(12) \quad {}_{40}V_1 = \begin{pmatrix} \frac{\partial h_1}{\partial b_1} & \frac{\partial h_2}{\partial b_1} & \dots \\ \frac{\partial h_1}{\partial b_2} & \frac{\partial h_2}{\partial b_2} & \dots \\ \dots & \dots & \dots \end{pmatrix}_{40 \times 10} \cdot \begin{pmatrix} \text{dh}_1 \\ \text{dh}_2 \\ \dots \end{pmatrix}_{10 \times 1} - \begin{pmatrix} \text{db}_1 \\ \text{db}_2 \\ \dots \end{pmatrix}_{40 \times 1}$$

The partial derivatives in the Jacobian matrix can easily be determined with

$$(13) \quad \frac{\partial h_i}{\partial b_k} = \frac{2 \cdot R_E}{b_k},$$

when R_E is the radius of the Earth and b_k is the length of the baseline k .

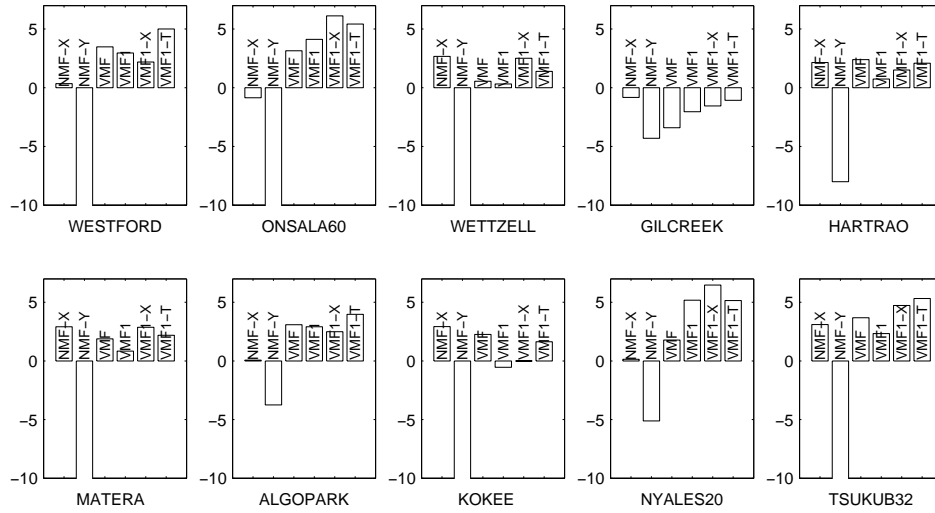


Figure 7. Changes of station heights in mm when using other mapping functions instead of NMF [Niell, 1996]. It is evident that with the hydrostatic NMF as total mapping function (denoted by NMF-Y) very poor results are obtained.

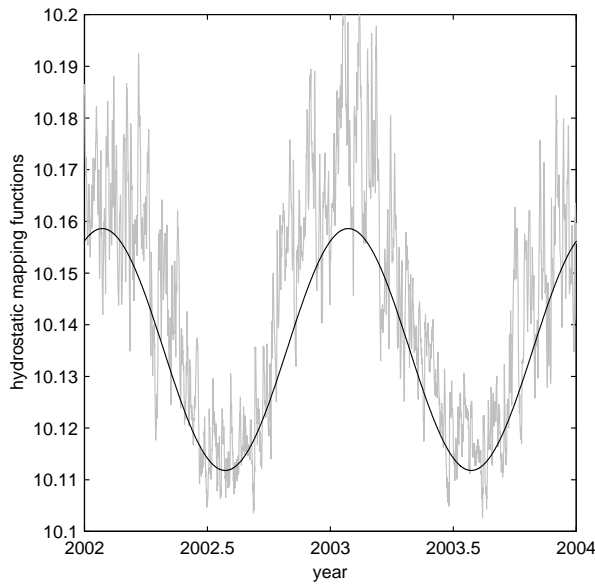


Figure 8. Hydrostatic mapping functions VMF (gray) and NMF (black) for 5° elevation at Algonquin Park (Canada) in 2002 and 2003.

Figure 7 shows the changes of the station heights determined from the changes of the mean baseline lengths (see equations 12 and 13) when using the various mapping functions instead of NMF [Niell, 1996]. The dominant feature in this plot is the change in baseline length when using the hydrostatic mapping function NMFh for the estimation of the total delays denoted by NMF-Y. This can be explained with the rule of thumb (see section 1), because the wet zenith delays are mapped down with the wrong mapping function. E.g., if there is a wet zenith

delay of 10 cm, the corresponding error in station height is 1.2 cm. Thus, the combination NMF-Y should never be used in GPS or VLBI analysis.

To illustrate the difference between NMF and VMF, the station Algonquin Park in Canada is used as example. As can be seen in figure 7, the station height increases by about 3 mm when using variations of VMF instead of NMF. Figure 8 shows the hydrostatic mapping function at 5° elevation for VMF and NMF in 2002 and 2003. Apart from a difference in the seasonal amplitude, a mean bias of about -0.01 can be seen between the hydrostatic mapping functions ($\text{NMFh} - \text{VMFh}$), which corresponds to a bias of about -2 cm between the hydrostatic delays at 5° elevation. Following the particularization of Niell's rule of thumb (see section 1), the corresponding station height change is 4 mm which is very close to the ~ 3 mm in figure 7.

Table 4 shows that there is a bias of -16 mm between the hydrostatic zenith delays determined from the observed pressure values at Wettzell and the hydrostatic zenith delays from ECMWF data. As indicated in section 3, this corresponds to a station height error of 2 mm for VMF1-X (compared to the VMF1 solution) if we assume the observed pressure values to be true, which is consistent with the bias shown in figure 7. To illustrate the biases between VMF and VMF1, the station Ny-Ålesund is chosen because it is situated rather close to the North pole (79° latitude) where the differences are larger than at mid-latitudes. Figure 2 shows that the differential hydrostatic delays at 5° elevation between VMF1 and VMF are -18 mm and 0 mm in January and July, respectively, corresponding to a mean difference of -9 mm over the year. Multiplied by 0.2 (the approximate ratio of the height error and the mapping function error at a 5° minimum elevation), this difference corresponds to a station height difference of ~ 2 mm, which is similar to the station height difference in figure 7 for Ny-Ålesund between VMF and VMF1. Similar assessments can be made for the stations Kokee Park and Hartebeesthoek.

5 Conclusions

The mapping functions NMF [Niell, 1996], IMF [Niell, 2000], and VMF [Boehm and Schuh, 2004] apply parameters for the b and c coefficients of the continued fraction form (equation 2) that are symmetric with regard to the equator (apart from the phase offset for the two hemispheres with NMF). In this paper it is shown that close to the equator and at high latitudes these coefficients have deficiencies, which could influence the mean station heights by as much as 4 mm. Therefore, new b and c coefficients have been developed from ERA-40 data in 2001 for the hydrostatic mapping function, and the corresponding mapping function is

referred to as VMF1. This VMF1 yields a small but significant improvement compared to the original VMF [Boehm and Schuh, 2004] as far as baseline length repeatabilities are concerned.

Using hydrostatic mapping functions as the partial derivatives for the estimation of total zenith delays distorts the baseline lengths considerably and thus, this approach should never be used. Alternatively, the concept of the Vienna Total Mapping Function VMF1-T is introduced which is not affected by bad a priori hydrostatic zenith delays but suffers significantly from poor a priori information about the wet part in the atmosphere. Thus, if observed pressure values are not available at the sites, VMF1-T should not be used, especially since better alternatives exist (VMF1-X).

It is shown that a priori hydrostatic zenith delays determined from raytracing through the ECMWF pressure level data can be used if no pressure values are available for a site, e.g. at GPS stations where pressure records often are not available. These a priori hydrostatic (and wet) zenith delays are provided at the webpage of the authors, <http://www.hg.tuwien.ac.at/~ecmwf>, for 213 IGS stations, together with the parameters of the Vienna Mapping Functions.

In the analyses of VLBI and GPS observations, there is always a trade-off between better separability of station heights, tropospheric zenith delays, and clock parameters on the one hand, and increasing mapping function errors on the other hand as observations at lower elevations are included [MacMillan and Ma, 1994]. New mapping functions, such as IMF, VMF, and VMF1 are required to reduce systematic errors, which is important to the geophysical use of geodesy, e.g. to detect signals in the coordinate time series that are related to hydrology. Since GPS is affected by a multitude of low-elevation error sources, such as poor or missing antenna phase center models for low elevations, the cutoff elevation angle is often set to 7° or even 10° . Then, although the differences between VMF and VMF1 might not be significant, the biases between VMF and NMF are expected to be still large enough to significantly change the station heights and, consequently, to influence the terrestrial reference frame.

Acknowledgements

We would like to thank the Austrian Science Fund FWF for supporting this work (P16992-N10), and we are very grateful to the two reviewers who gave valuable advices to the

manuscript. In particular, we want to thank Arthur Niell who pointed out the deficiencies of the total mapping function.

References

Berg, H., Allgemeine Meteorologie, Duemmler's Verlag, Bonn, 1948.

Boehm, J., and H. Schuh, Vienna Mapping Functions in VLBI analyses , Geophys. Res. Lett., 31, L01603, doi:10.1029/2003GL018984, 2004.

Boehm, J., Troposphärische Laufzeitverzögerungen in der VLBI, Veröffentlichung des Institutes für Geodäsie und Geophysik, Geowissenschaftliche Mitteilungen, Heft Nr. 68, ISSN 1811-8380, 2004.

Chao, C.C., The troposphere calibration model for Mariner Mars 1971, JPL Technical Report 32-1587, NASA JPL, Pasadena CA, 1974.

Davis, J.L, T.A. Herring, I.I. Shapiro, A.E.E. Rogers, and G. Elgered, Geodesy by Radio Interferometry: Effects of Atmospheric Modeling Errors on Estimates of Baseline Length, Radio Science, Vol. 20, No. 6, pp. 1593-1607, 1985.

Eanes, R.J., Diurnal and Semidiurnal tides from TOPEX/POSEIDON altimetry. Eos Trans. AGU, 75(16):108, 1994.

Hugentobler, U., S. Schaer, and P. Fridez, Bernese GPS Software Version 4.2, Astronomical Institute of the University of Berne, 2001.

Koch, K.R., Parameter Estimation and Hypothesis Testing in Linear Models, Springer, Berlin, 1999.

MacMillan, D.S., and C. Ma, Evaluation of very long baseline interferometry atmospheric modeling improvements, J. Geophys. Res., 99, B1, pp. 637-651, 1994.

MacMillan, D.S., and C. Ma, Using Meteorological Data Assimilation Models in Computing Tropospheric Delays at Microwave Frequencies, Phys. Chem. Earth, Vol. 23, No. 1, pp. 97-102, 1998.

Marini, J.W., Correction of satellite tracking data for an arbitrary tropospheric profile, Radio Science, Vol. 7, No. 2, pp. 223-231, 1972.

Niell, A.E., Global mapping functions for the atmosphere delay at radio wavelengths, J. Geophys. Res., 101, B2, pp. 3227-3246, 1996.

Niell, A.E., Improved atmospheric mapping functions for VLBI and GPS, Earth Planets Space, 52, pp. 699-702, 2000.

Niell, A.E., A.J. Coster, F.S. Solheim, V.B. Mendes, P.C. Toor, R.B. Langley, and C.A. Upham, Comparison of Measurements of Atmospheric Wet Delay by Radiosonde, Water Vapor Radiometer, GPS and VLBI, *Journal of Atmospheric and Oceanic Technology*, 18, pp. 830-850, 2001.

Niell, A.E., and L. Petrov, Using a Numerical Weather Model to Improve Geodesy, in *Proceedings: The State of GPS Vertical Positioning Precision: Separation of Earth Processes by Space Geodesy*, April 2-4, 2003, Luxembourg, 2003.

Petrov, L., and J.P. Boy, Study of atmospheric pressure loading signal in VLBI observations, *Journal of Geophysical Research*, 10.1029/2003JB002500, 2003.

Saastamoinen, J., Contributions to the Theory of Atmospheric Refraction, Part II, *Bulletin Geodesique*, Vol. 107, pp. 13-34, 1973.

Snajdrova, K., J. Boehm, P. Willis, R. Haas, and H. Schuh, Multi-technique comparison of tropospheric zenith delays derived during the CONT02 campaign, accepted by *Journal of Geodesy*, 2005.

Scherneck, H.-G., and M.S. Bos, Ocean Tide and Atmospheric Loading, *International VLBI Service for Geodesy and Astrometry 2002 General Meeting Proceedings*, edited by Nancy R. Vandenberg and Karen D. Baver, NASA/CP-2002-210002, 205-214, 2002.

Simmons, A.J., and J.K. Gibson (editors), The ERA-40 Project Plan, ERA-40 Project Report Series No. 1, <http://www.ecmwf.int>, 2000.

Thomas, C., and D.S. MacMillan, Core Operation Center Report, in *International VLBI Service for Geodesy and Astrometry 2002 Annual Report*, edited by N. R. Vandenberg and K. D. Baver, NASA/TP-2003-211619, 2003.

Titov, O., V. Tesmer, and J. Boehm, Occam Version 5.0 Software User Guide, AUSLIG Technical Report 7, 2001.

Johannes Böhm, Arthur Niell, Paul Tregoning, and Harald Schuh

Global Mapping Function (GMF):

A new empirical mapping function based on numerical weather model data

Geophysical Research Letters

Vol. 33, L07304, doi:10.1029/2005GL02554

2006b

The Global Mapping Function (GMF):

A new empirical mapping function based on numerical weather model data

Johannes Böhm, Arthur Niell, Paul Tregoning, and Harald Schuh

Abstract

Troposphere mapping functions are used in the analyses of Global Positioning System and Very Long Baseline Interferometry observations to map a priori zenith hydrostatic and wet delays to any elevation angle. Most analysts use the Niell Mapping Function (NMF) whose coefficients are determined from site coordinates and the day of year. Here we present the Global Mapping Function (GMF), based on data from the global ECMWF numerical weather model. The coefficients of the GMF were obtained from an expansion of the Vienna Mapping Function (VMF1) parameters into spherical harmonics on a global grid. Similar to NMF, the values of the coefficients require only the station coordinates and the day of year as input parameters. Compared to the 6-hourly values of the VMF1 a slight degradation in short-term precision occurs using the empirical GMF. However, the regional height biases and annual errors of NMF are significantly reduced with GMF.

1. Introduction

For space geodetic measurements, estimates of atmosphere delays are highly correlated with site coordinates and receiver clock biases. Thus it is important to use the most accurate models for the atmosphere delay to reduce errors in the estimates of the other parameters. Numerical Weather Models (NWM) provide the spatial distribution of refractivity throughout the troposphere with high temporal resolution for mapping the zenith troposphere delay to the elevation of each observation by so-called mapping functions. The information needed for the mapping functions must be obtained from an external source, i.e. the NWM, prior to geodetic data analysis. In contrast, the Niell Mapping Function (NMF) was built on one year of radiosonde profiles from the northern hemisphere [Niell, 1996]; the spatial and temporal variability of the mapping function is accounted for with only a latitude and seasonal dependence. This empirical approach considerably simplifies the estimation process since no external data are required. However, following the development of NMF, two deficiencies became evident: a) latitude-dependent biases, which are largest in high southern latitudes, and

b) the lack of sensitivity to the longitude of a site, what causes systematic distortions of estimated positions in some areas, for example over northeast China and Japan. The simple temporal and latitudinal functions of the NMF do not provide the resolution to capture the higher variability in space and time that are seen in mapping functions based on NWM data [Boehm and Schuh, 2004; Boehm *et al.*, 2006].

Boehm *et al.* [2006] showed from an analysis of Very Long Baseline Interferometry (VLBI) observations that the application of the Vienna Mapping Function (VMF1), with coefficients given at 6-hourly time intervals, considerably improves the precision of geodetic results such as baseline lengths and station heights. VMF1 is currently the mapping function providing globally the most accurate and reliable geodetic results. Moreover, systematic station height changes of up to 10 mm occur when changing from the NMF to the VMF1.

The goal of this paper is to present a mapping function which can be used globally and implemented easily in existing geodetic analysis software and which provides consistency with NWM-based mapping functions, in particular with the VMF1 [Boehm *et al.*, 2006]. The parameterization of the coefficients in the three-term continued fraction (see Equation (1)) that is used in most mapping functions has been refined to include a dependence on longitude. The accuracies of the mapping functions have been improved by extending the temporal range of input data used and also by global sampling of the atmosphere by raytracing through a global NWM instead of the limited number of radiosonde sites used to derive the NMF. The resulting mapping functions, one each for the hydrostatic and wet components, are designated the Global Mapping Function (GMF).

We compare the empirical GMF with mapping functions derived from radiosonde data, with NMF, and with VMF1.

2. Mapping Functions

For space geodetic measurements it is convenient to characterize the azimuthally symmetric component of the atmospheric delay with a value in the zenith direction that varies with time on a scale of twenty minutes to a few hours. The delay in the direction of an observation is related to the zenith delay by a mapping function, which is modelled with sufficient accuracy for elevations down to 3° using a three term continued fraction in $\sin e$ elevation, e , [Niell, 1996] given by:

$$(1) \quad mf(e) = \frac{1 + \frac{a}{1 + \frac{b}{1 + c}}}{\sin e + \frac{a}{\sin e + \frac{b}{\sin e + c}}}$$

The parameters a , b , and c are different for the hydrostatic and wet components of the atmosphere designated with indices h or w in section 3. They should be related with sufficient accuracy to the characteristics of the atmosphere at the time of observation to avoid introducing significant error into the estimation of the geodetic site coordinates. For NMF [Niell, 1996], each of the parameters is a constant or a function of site latitude (symmetric about the equator) and day of year. Thus, only the seasonal dependence of the temporal variation of the atmosphere is taken into account. The mapping functions IMF [Niell, 2001] and VMF1 [Boehm *et al.*, 2006] use the output of a numerical weather analysis to provide information specifically for the geographic location of the site with a temporal resolution of six hours. They differ in the ease of computation of the parameters and the amount of data used from the NWM. While VMF1 is more accurate, IMF is more generally applicable. The accuracy improvement over NMF is especially significant for the hydrostatic component for both VMF1 and IMF.

Different mapping functions produce different coordinate estimates, not only in terms of precision and repeatability but also with different biases and seasonal variability. It is necessary to use consistent mapping functions for all analyses in order to derive consistent sets of coordinates. The VMF1 is provided only at discrete locations, e.g. all IVS (International VLBI Service for Geodesy and Astrometry) sites and all IGS (International GNSS Service) sites, and does not cover the whole time period of global GPS observations since the early 1990s. Therefore, it is desirable to have a mapping function compatible with NMF, that can be computed empirically for any site at any date but which is more consistent with the VMF1 than is NMF. Such a mapping function could be seen as a back-up in case the NWM-based models are not available for some period of time or are discontinued.

3. Determination of the Global Mapping Function (GMF)

Using $15^\circ \times 15^\circ$ global grids of monthly mean profiles for pressure, temperature, and humidity from the ECMWF (European Centre for Medium-Range Weather Forecasts) 40 years reanalysis data (ERA40), the coefficients a_h and a_w were determined for the period

September 1999 to August 2002 applying the same strategy which was used for VMF1. Taking empirical equations for b and c (from VMF1) the parameters a were derived by a single raytrace at 3.3° initial elevation angle [Boehm *et al.*, 2006]. Thus, at each of the 312 grid points, 36 monthly values were obtained for the hydrostatic and wet a parameters. The hydrostatic coefficients were reduced to mean sea level by applying the height correction given by Niell [1996]. The mean values, a_0 , and the annual amplitudes A of a sinusoidal function (Equation (2)) were fitted to the time series of the a parameters at each grid point, with the phases referred to January 28, corresponding to the NMF. The standard deviations of the monthly values at the single grid points with respect to Equation (2) increase towards higher latitude from the equator, with a maximum value of 8 mm (equivalent station height error) in Siberia. For the wet component, the standard deviations are smaller with maximum values of about 3 mm at the equator.

$$(2) \quad a = a_0 + A \cdot \cos\left(\frac{\text{doy} - 28}{365} \cdot 2\pi\right)$$

$$(3) \quad a_0 = \sum_{n=0}^9 \sum_{m=0}^n P_{nm}(\sin \varphi) \cdot [A_{nm} \cdot \cos(m \cdot \lambda) + B_{nm} \cdot \sin(m \cdot \lambda)]$$

Then, the global grid of the mean values a_0 and that of the amplitudes A for both the hydrostatic and wet coefficients of the continued fraction form were expanded into spatial spherical harmonic coefficients up to degree and order 9 (according to Equation (3) for a_0) in a least-squares adjustment. The residuals of the global grid of a_0 and A values to the spherical harmonics are in the sub-millimeter range (in terms of station height). The hydrostatic and wet coefficients a for any site coordinates and day of year can then be determined using Equation (2).

4. Validation and comparison of mapping functions

4.1 Validation of mapping functions with radiosondes

The most accurate computation of azimuthally symmetric mapping functions is assumed to be obtained from vertical profiles of temperature, pressure, and humidity from radiosondes [Niell *et al.*, 2001]. The mapping function is then computed as the ratio of the delay (obtained by

raytracing) along the path at the desired elevation to the delay in the zenith direction. For convenience we compare the mapping functions for a vacuum (outgoing) elevation angle of 5° . The radiosonde data used for this comparison are from 23 sites and span the latitude range from -66° to $+75^\circ$. However, it has to be mentioned that the majority of the radiosonde sites are in the northern hemisphere. A 'rule of thumb' [MacMillan and Ma, 1994] states that for azimuthally symmetric delay errors and observations down to approximately 5° , the height error is approximately one fifth of the delay error at the lowest elevation. The mapping function differences have been converted to an equivalent height difference using this rule of thumb because station height changes are more easily visualized than differences in the a coefficients. The mean station height differences, averaged over the year, are shown in Figure 1 after comparing the hydrostatic delays from NMF, GMF, and VMF1 with radiosonde data. The most important feature is the significantly smaller bias for hydrostatic GMF compared to hydrostatic NMF, thus confirming that the mean biases can be reduced with GMF. On the other hand, GMF and NMF are not significantly different with respect to the standard deviations of the height changes (not shown here) since both contain only annual time variability, whereas the actual variations occur on weekly, daily, and sub-daily time scales. The influence of the wet mapping functions is less critical than the hydrostatic component in GPS and VLBI analyses, since the wet delays are typically smaller than the hydrostatic delays by a factor of 10.

4.2 NMF and GMF compared to VMF1 in GPS analysis

A global network of more than 100 GPS stations was analysed with the software package GAMIT Version 10.21 [King and Bock, 2005; Herring, 2005] applying the NMF, GMF, and VMF1 mapping functions. We processed observations from July 2004 through June 2005, producing a fiducial-free global network for each day. The elevation cutoff angle was set to 7° and no downweighting of low observations was applied to make the performance of the mapping functions most visible. Atmospheric pressure loading (tidal and non-tidal) [Tregoning and van Dam, 2005] was applied along with ocean tide loading and the IERS2003 solid Earth tide model [IERS Conventions 2003]. We estimated satellite orbital parameters, station coordinates, zenith tropospheric delay parameters every 2 hours, and resolved ambiguities where possible. We used ~ 60 sites to transform the fiducial-free networks into the ITRF2000 by estimating 6-parameter transformations (3 rotations, 3 translations) [Herring 2005]. For the investigations described below the time series were used of those 133 stations

which have more than 300 daily height estimates. The latitudes of the sites are indicated in Figure 2 which shows the mean changes of GPS station heights with NMF or GMF relative to using VMF1. It is evident that the agreement between VMF1 and GMF is very good, whereas station height differences up to 10 mm occur in the southern hemisphere south of 45° S and in the Japan region when changing from VMF1 to NMF.

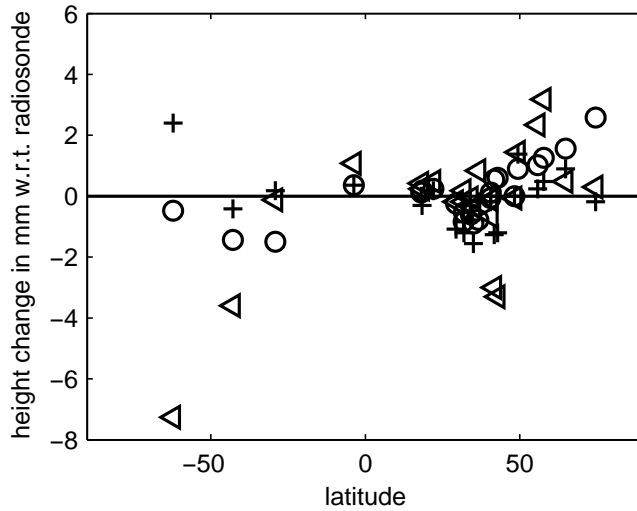


Figure 1: Mean height differences in mm for hydrostatic NMF (\triangle), GMF (+), and VMF1 (o) relative to radiosonde based mapping functions for 1992.

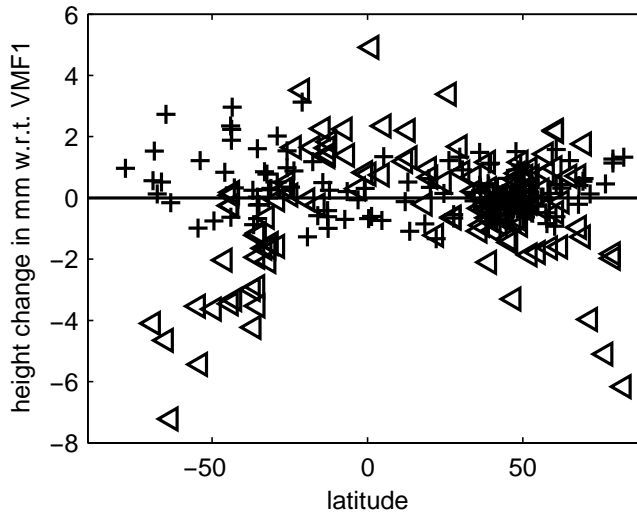


Figure 2: Mean height changes in mm when using NMF (\triangle) and GMF (+) in GPS analysis with heights obtained with VMF1 as reference.

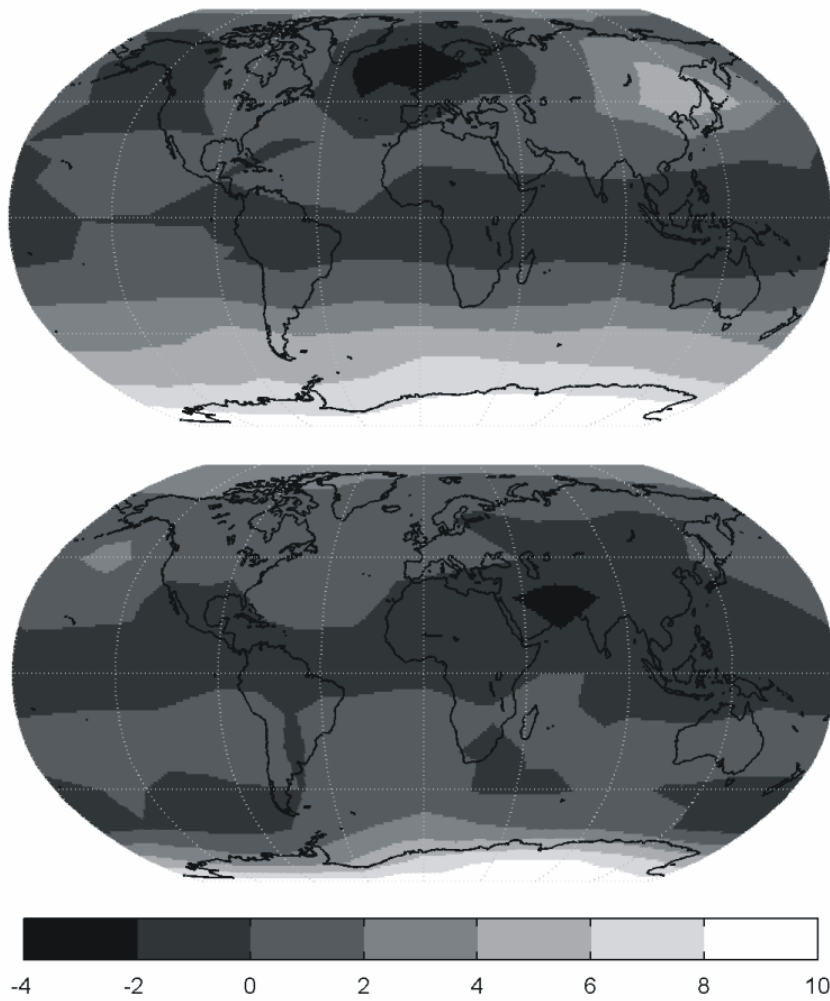


Figure 3: Mean height changes (in mm) when using the hydrostatic GMF instead of NMF for January (upper plot) and July (lower plot) determined by applying the rule of thumb. The largest differences can be found in January south of 45° S and in northeast China and Japan, with station height differences up to 10 mm.

4.3 NMF versus GMF

Computing hydrostatic GMF and NMF for each month on a global grid and applying the rule of thumb, we derived corresponding station height differences. In Figure 3 the height changes from NMF to GMF are plotted for January and July. These comparisons show that there is pretty good agreement between NMF and GMF in July (apart from Antarctica), but that in January differences are large (up to 15 mm) south of 45° S and in northeast China and Japan. These height changes vary throughout the year and influence other parameters such as scale and geocenter motion.

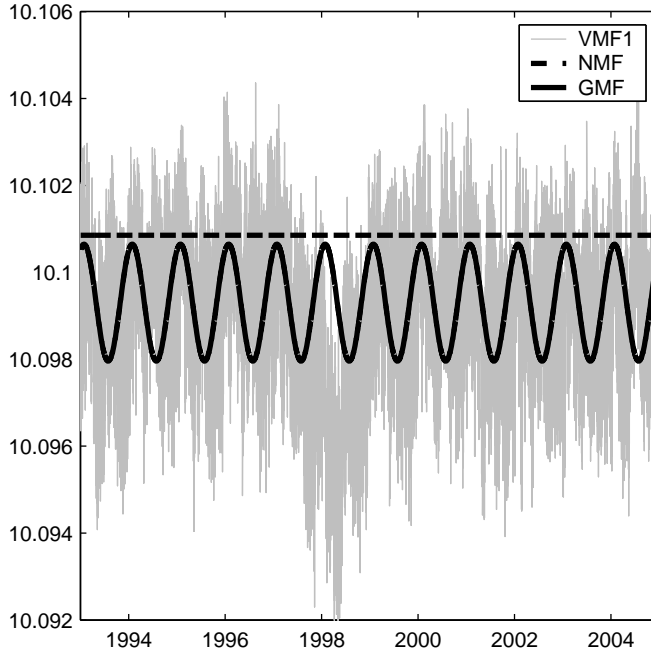


Figure 4: Hydrostatic mapping function at 5° elevation at Fortaleza, Brazil. Phenomena such as the El Niño event in 1997 and 1998 cannot be accounted for with empirical mapping functions like NMF or GMF that contain only average seasonal terms.

In Figure 4 the three hydrostatic mapping functions discussed in this paper at 5° elevation are plotted for Fortaleza, Brazil. The NMF does not show a seasonal variation because this station is situated near the equator (2° S). In contrast, the GMF reflects a seasonal variability and, on average, agrees much better with the VMF1. However, a deficiency is evident in both empirical mapping functions compared to the VMF1 because neither NMF nor GMF reveal the unusual meteorological conditions described by the VMF1 during the El Niño phenomena in 1997 and 1998.

5. Conclusions

To achieve the highest accuracy in VLBI and GPS analyses, it is recommended to use troposphere mapping functions that are based on data from numerical weather models. Today, these mapping functions (e.g. VMF1 [Boehm *et al.*, 2006] or IMF [Niell, 2001]) are available as time series of coefficients with a resolution of six hours. However, for particular time periods or stations where NWM-based mapping functions are not available, the GMF can be used without introducing systematic biases in the coordinate time series, although the short-term precision will suffer compared to the VMF1. The GMF can serve as a 'back-up' mapping function or a compatible empirical representation of the more complex NWM-based mapping

functions. The GMF provides better precision than the NMF and smaller height biases with respect to VMF1. It can be implemented very easily because it uses the same input parameters (station coordinates and day of year) as NMF, which is already implemented in most space geodesy software packages. Code for *FORTRAN* implementations of VMF1 and GMF are provided at <http://www.hg.tuwien.ac.at/~ecmwf1>, as are the input data for VMF1 and IMF.

Acknowledgments

We would like to thank the Zentralanstalt für Meteorologie und Geodynamik (ZAMG) for allowing us access to the data of the European Centre for Medium-Range Weather Forecasts (ECMWF). Johannes Boehm and Harald Schuh are grateful to the Austrian Science Fund (FWF) for supporting this work under project P16992-N10. Arthur Niell was supported by NASA contract NNG05HY03C. The GPS analyses were computed on the Terrawulf linux cluster belonging to the Centre for Advanced Data Inference at the Research School of Earth Sciences, The Australian National University.

References

- Boehm J., and H. Schuh (2004), Vienna Mapping Functions in VLBI analyses, *Geophys. Res. Lett.* 31(1):L01603, DOI:10.1029/2003GL018984.
- Boehm J., B. Werl, and H. Schuh (2006), Troposphere mapping functions for GPS and VLBI from ECMWF operational analysis data, *Journal of Geophysical Research*, *in press*.
- Herring, T.A. (2005), GLOBK Global Kalman Filter VLBI and GPS analysis program, version 10.1, *Mass. Inst. of Technol.*, Cambridge, MA.
- King, R.W., and Y. Bock (2005), Documentation for the GAMIT GPS processing software Release 10.2, *Mass. Inst. of Technol.*, Cambridge, MA.
- MacMillan, D.S., and C. Ma (1994), Evaluation of very long baseline interferometry atmospheric modeling improvements, *J. Geophys. Res.*, 99, B1, pp. 637-651.
- McCarthy, D.D., and G. Petit (2004). IERS Conventions (2003), IERS Technical Note, No. 32, Verlag des Bundesamtes für Kartographie und Geodäsie, Frankfurt am Main.
- Niell, A.E. (1996), Global mapping functions for the atmosphere delay at radio wavelengths, *J. Geophys. Res.* 101(B2):3227-3246.
- Niell, A. E. (2001), Preliminary evaluation of atmospheric mapping functions based on numerical weather models, *Phys. Chem. Earth*, 26, 475-480.

Niell A.E., A.J. Coster, F.S. Solheim, V.B. Mendes, P.C. Toor, R.B. Langley, C.A. Upham (2001), Comparison of Measurements of Atmospheric Wet Delay by Radiosonde, Water Vapor Radiometer, GPS, and VLBI, *Journal of Atmospheric and Oceanic Technology* 18:830-850.

Tregoning, P., and T. van Dam (2005), Atmospheric pressure loading corrections applied to GPS data at the observation level, *Geophys. Res. Lett.*, 32, L22310, doi:10.1029/2005GL024104.

Johannes Böhm, Robert Heinkelmann, and Harald Schuh

Short Note:

A Global Model of Pressure and Temperature for Geodetic Applications

Journal of Geodesy

doi:10.1007/s00190-007-0135-3

2007a

Short Note:**A Global Model of Pressure and Temperature for Geodetic Applications**

Johannes Böhm, Robert Heinkelmann, and Harald Schuh

Abstract

The empirical model GPT (Global Pressure and Temperature), which is based on spherical harmonics up to degree and order nine, provides pressure and temperature at any site in the vicinity of the Earth's surface. It can be used for geodetic applications such as the determination of a priori hydrostatic zenith delays, reference pressure values for atmospheric loading, or thermal deformation of Very Long Baseline Interferometry (VLBI) radio telescopes. Input parameters of GPT are the station coordinates and the day of the year, thus also allowing one to model the annual variations of the parameters. As an improvement compared to previous models, it reproduces the large pressure anomaly over Antarctica, which can cause station height errors in the analysis of space geodetic data of up to one centimetre if not considered properly in troposphere modelling. First tests at selected geodetic observing stations show that the pressure biases considerably decrease when using GPT instead of the very simple approaches applied in various Global Navigation Satellite Systems (GNSS) software packages so far. GPT also provides an appropriate model of the annual variability of global temperature.

Keywords: GNSS, VLBI, neutral atmosphere delays

1 Introduction

In the analysis of Global Navigation Satellite System (GNSS) and Very Long Baseline Interferometry (VLBI) observations, accurate a priori hydrostatic zenith delays must be used. Preferably, they are determined from pressure values recorded at the sites (Saastamoinen 1972), but they can also be derived from numerical weather models (NWM), although with some loss of accuracy. For example, hydrostatic zenith delays are provided with the coefficients of the NWM-based Vienna Mapping Function 1 (Boehm et al. 2006a). If neither of these two data streams is accessible, a standard model for the pressure is often used. To provide precise and un-biased global pressure values, we have derived the empirical model

GPT (Global Pressure and Temperature) which describes the annual variation of the pressure at the Earth surface and which agrees with mean pressure values so that no systematic station height errors are introduced.

The pressure values calculated from GPT can also be entered into atmosphere pressure loading models as reference pressure, whereas the temperature values can be used for determining annual thermal deformations of radio telescopes (or for buildings with GNSS antennas on top of them) or as reference temperatures for these thermal deformations, respectively. Finally, as a by-product, GPT yields rough estimates for global geoid undulations.

2 Determination of GPT

In terms of mathematics and the underlying meteorological data, the determination of GPT is similar to the development of the empirical Global Mapping Function (GMF) (Boehm et al. 2006b), i.e., it is based on three years (September 1999 to August 2002) of $15^\circ \times 15^\circ$ global grids of monthly mean profiles for pressure and temperature from the ECMWF (European Centre for Medium-Range Weather Forecasts) 40 years reanalysis data (ERA40, Uppala et al. 2005). The corresponding grid of orthometric heights H of the Earth surface with respect to mean sea level is also available from the ECMWF.

In a first step, for each vertical profile, the pressure and temperature values are determined for the Earth surface by interpolating exponentially and linearly, respectively. Then, the pressure values p on the Earth surface at height h are reduced to pressure values p_r at mean sea level h_r (Eq. 1, Berg 1948) and a linear decrease of temperature T with height is assumed (Eq. 2).

$$(1) \quad p = p_r \cdot (1 - 0.0000226 \cdot (h - h_r))^{5.225}$$

$$(2) \quad dT/dh = -0.0065^\circ\text{C}/\text{m}$$

Thus for each grid point 36 monthly mean values of pressure and temperature at mean sea level are available. For these two series the mean values, a_0 , and the annual amplitudes, A , are estimated with the phase offset fixed to January 28 (Niell 1996) when *doy* is the day of the year.

$$(3) \quad a = a_0 + A \cdot \cos\left(\frac{\text{doy} - 28}{365.25} \cdot 2\pi\right)$$

The residuals to this model are as large as 20 hPa for the pressure and 10 °C for the temperature at higher latitudes; they are significantly smaller at the equator, consistent with the meteorological variability (Fig. 1).

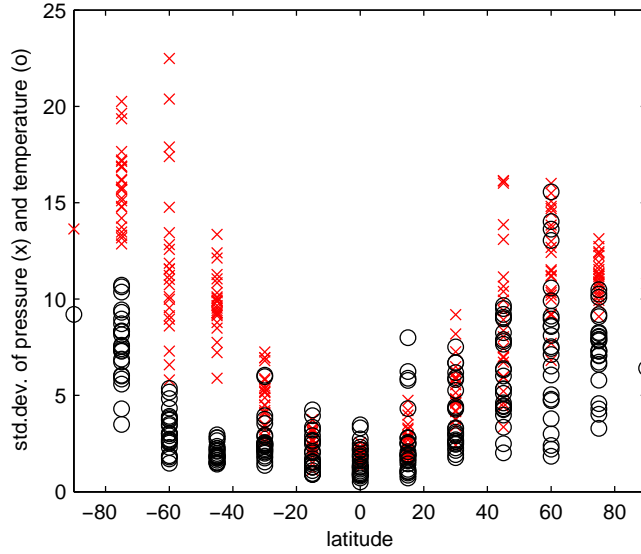


Figure 1. Standard deviation of residuals to the annual model for pressure [hPa] (x) and temperature [°C] (o) with respect to latitude.

In the next step, each of the four grids (mean values at mean sea level and annual amplitudes of pressure and temperature) is expanded into spherical harmonics up to degree and order nine (as an example see Eq. 4 for the grid of mean values, a_0). The P_{nm} are the Legendre polynomials (Heiskanen and Moritz 1967, p. 22), φ and λ are latitude and longitude, and A_{nm} and B_{nm} are the coefficients for degree n and order m which are determined within a least-squares adjustment.

$$(4) \quad a_0 = \sum_{n=0}^9 \sum_{m=0}^n P_{nm}(\sin \varphi) \cdot [A_{nm} \cos(m\lambda) + B_{nm} \sin(m\lambda)]$$

GPT uses Eq. (4) to derive the mean value, a_0 , and a similar equation for amplitude, A , which are then entered into Eq. (3) together with the day of the year to get the pressure or the temperature at mean sea level. Constant reference values for pressure and temperature (yearly means) can be derived from Eq. (3) if $(28 + 365.25/4)$ is used as day of the year. To determine

the pressure and temperature at the site, the orthometric height H should be used together with Eq. (1) and (2), respectively. However, since the orthometric heights of the stations are often not accessible for the user, GPT accepts ellipsoidal height as input. To accommodate this the geoidal undulations N from the EGM96 model (Lemoine et al. 1998) have been expanded into spherical harmonics up to degree and order nine and are used to transform the ellipsoidal heights h to orthometric heights H ($h = H + N$). The geoidal undulation N can be as large as 100 m (approximately 12 hPa); applying a rule of thumb (e.g. MacMillan and Ma 1994), an error of the pressure value of 12 hPa used in the troposphere model corresponds to a station height error of approximately 3 mm.

3 Validation of GPT

In the Bernese software package (BSW, Hugentobler et al. 2006) Eq. (1) by Berg (1948) is used together with the reference pressure $p_r = 1013.25$ hPa at the ellipsoid to determine the pressure p at the site which is then used to calculate the a priori hydrostatic zenith delay (Saastamoinen 1972). In the GAMIT software (King and Bock 2006) Eq. (5) by Hopfield (1969) is applied with the atmospheric temperature $T_k = 293.16$ K, the normal lapse rate of temperature with height $\alpha = 4.5$ K/km, the gravity at the surface of the Earth $g = 9.7867$ m/s², the gas constant for dry air $R = 0.287$ kJ/K/kg, and also the reference pressure $p_r = 1013.25$ hPa at the ellipsoid.

$$(5) \quad p = p_r \cdot \left(\frac{T_k - \alpha \cdot h}{T_k} \right)^{(g/R\alpha)}$$

Fig. 2 shows by latitude band the mean values and standard deviations of the differences of pressure derived from GPT and pressure determined with the models by Berg and Hopfield (both assuming 1013.25 hPa at the ellipsoid). Most striking is the significant decrease of the pressure towards the South Pole which is modelled by GPT but cannot be accounted for by the models Berg and Hopfield because of two reasons: (1) Low mean sea level pressure is dominating at the coast of the Antarctica (Uppala et al. 2005); (2) Although the vertical gradient of the pressure is dependent on the temperature, the models by Berg and Hopfield (as implemented in GAMIT) imply constant values for the temperature and temperature lapse rates. This weakness is even more important for Antarctica because the heights can be as large as 3 km. GPT also uses a constant pressure gradient (Eq. 1) but the extrapolation of the

pressure gets started at the mean Earth surface and not at the ellipsoid as it is the case with the models by Berg and Hopfield. Similar differences as shown in Fig. 2 have also been found by Tregoning and Herring (2006).

A pressure difference of 40 hPa as shown in Fig. 2 for the South Pole causes an apparent station height change in the geodetic analysis of more than 10 mm. However, since the slope of the pressure differences towards the South Pole is so distinct and the difference of 40 hPa is so large, we performed an independent comparison with monthly mean local pressure measurements in 1998 at the South Pole provided by the NOAA (National Oceanic and Atmospheric Administration, U.S.A.). Fig. 3 shows these monthly mean values of observed pressure values together with GPT and the Berg model, and it clearly confirms the pressure anomaly shown in Fig. 2. As we want to confirm these results with other independent observations, i.e. not with data retrieved from the ECMWF, recorded pressure values have been extracted from the VLBI databases. Fig. 4 shows these meteorological observations for station O'Higgins in Antarctica (-63° latitude, -58° eastern longitude) in comparison with GPT and the Berg model from year 2000 until 2005. Additionally, surface pressure values from the ECMWF given at 6 hour time intervals are plotted. It is evident that the recorded values at the station agree well with data from the ECMWF and are well represented by GPT, but that the model by Berg (Eq. 1) assuming 1013.25 hPa on the ellipsoid differs by approximately -15 hPa. This pressure difference at O'Higgins between GPT and the model by Berg is different from the mean values per latitude shown in Fig. 1 because there is also a large variation with longitude in this region.

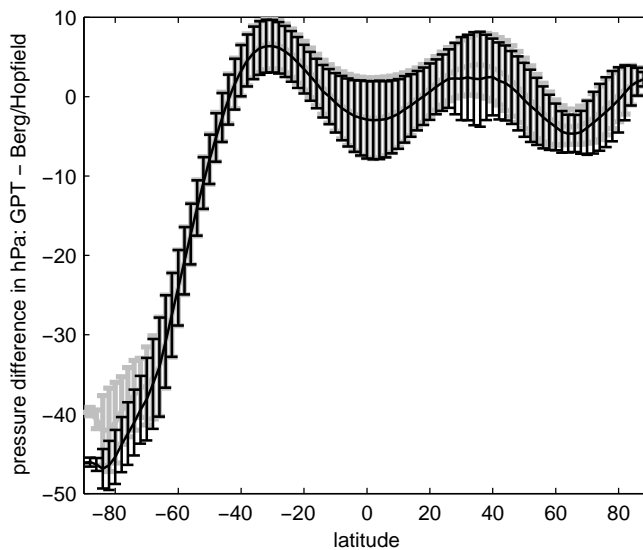


Figure 2. Pressure differences in hPa between GPT and the models by Berg (Eq. 1, grey error bars) and Hopfield (Eq. 3, black error bars) assuming 1013.25 hPa at the ellipsoid.

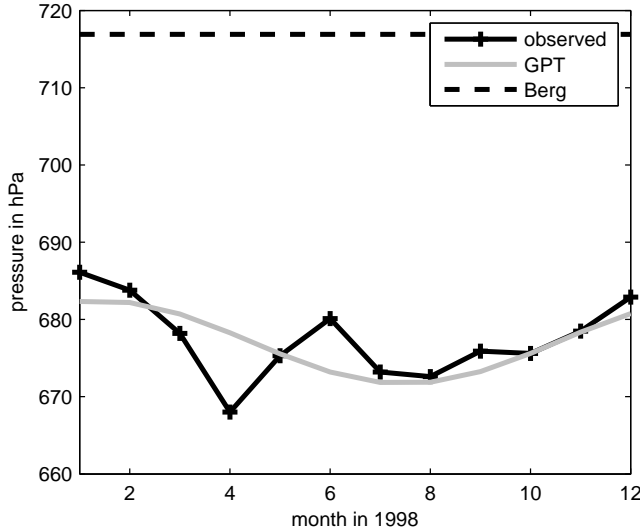


Figure 3. Monthly mean pressure values in 1998 observed at the South Pole (+), and the corresponding values from GPT (grey line) and the Berg model (dashed line).

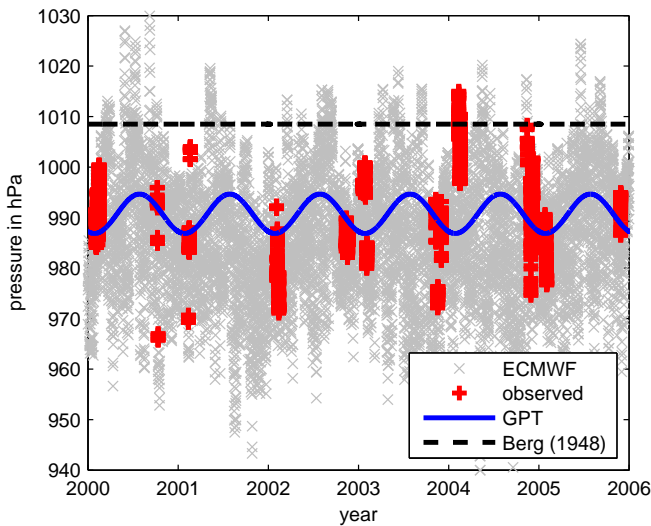


Figure 4. Pressure values for station O'Higgins in Antarctica from the ECMWF (x), pressure recordings at the radio telescope (+), GPT (-), and pressure determined with Eq. (1) (--).

Analogously, Fig. 5 shows the temperature values for O'Higgins. Unlike the pressure, there is a relatively large annual variation of the temperature which again is nicely represented by GPT.

Table 1 summarizes the biases and standard deviations between the recorded pressure and temperature values at six frequently observing VLBI radio telescopes and the modelled values for pressure from GPT and Eq. (1) and temperature from GPT and Eq. (2) (assuming a reference temperature of 15 °C at mean sea level). (It should be noted that the recorded pressure and temperature values are available only during the VLBI sessions, i.e. for about

one or two days per week.) Table 1 shows that the pressure bias is significantly reduced from Eq. (1) to GPT for four out of six stations. In particular the three largest biases get clearly smaller (Hartebeesthoek from 11.0 to 2.8 hPa, Kokee Park from 8.6 to 4.4 hPa, Wettzell from 10.8 to 2.7 hPa). The maximum bias for GPT is obtained at Algonquin Park with 5.7 hPa, which corresponds to a station height error of about 1.5 mm. On the other hand, there is no reduction of the standard deviation of the pressure, which is due to the fact that short term variations of the pressure (e.g. within a couple of days) far exceed the effect of annual pressure variations. This is different for the temperature where a clear improvement of the standard deviations is obtained if the annual variation is taken into account: As can be seen from the two last columns of Table 1, for three stations the standard deviations decrease by more than 40% with the new GPT model.

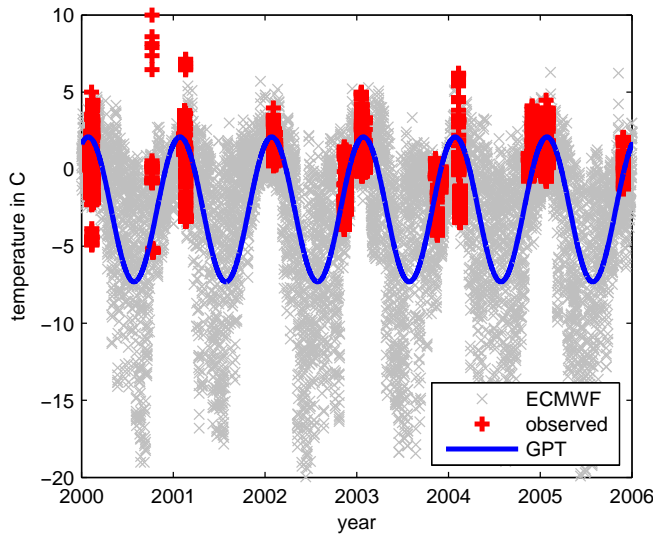


Figure 5. Temperature values for station O'Higgins in Antarctica from the ECMWF (x), temperature recordings at the radio telescope (+), and GPT (-).

Conclusions

It frequently happens in space-geodetic techniques data analyses that neither observed (recorded) pressure values nor values from a NWM are available to determine the hydrostatic zenith delays. In those instances we recommend the use of GPT for troposphere modelling in GNSS or VLBI analyses instead of taking simple models like the one given in Eq. (1). GPT can be easily implemented in any software package, and a combination of GPT with GMF (Boehm et al. 2006b) is useful. Because it is an empirical model, GPT can be used to define reference values for the pressure and temperature for other geodetic applications, such as

atmosphere loading or thermal deformations of VLBI radio telescopes. Future improvements of GPT might consider an increase of degree and order of the spherical harmonics expansion, however, such an update should be consistently done with an update of the Global Mapping Functions (GMF). GPT can be downloaded from <http://www.hg.tuwien.ac.at/~ecmwf1> .

Table 1. Biases and standard deviations between pressure and temperature values recorded at VLBI radio telescopes in 2005, and those determined either with GPT or Eq. (1) and (2) (Berg, 1948). For the comparison of the temperatures in the last column, 15 °C is used as reference value at mean sea level.

	latitude [°]	pressure [hPa] rec. – GPT	pressure [hPa] rec. – Berg	temp. [°C] rec. – GPT	temp. [°C] rec. – Eq. 2
Algonquin Park	46	5.7 ± 7.4	2.9 ± 7.3	0.5 ± 7.2	-10.2 ± 13.6
Hartebeesthoek	-26	2.8 ± 3.4	11.0 ± 3.7	0.3 ± 6.2	8.8 ± 6.4
Kokee Park	22	4.4 ± 2.3	8.6 ± 2.3	-0.3 ± 2.6	6.5 ± 2.8
Ny-Ålesund	78	0.7 ± 12.9	-2.9 ± 12.7	0.0 ± 5.4	-20.3 ± 5.9
Westford	49	1.2 ± 7.4	-0.5 ± 7.4	2.3 ± 5.8	-4.9 ± 10.9
Wettzell	42	2.7 ± 7.1	10.8 ± 7.0	0.3 ± 4.8	-4.9 ± 8.4

Acknowledgement

The authors would like to thank the *Zentralanstalt für Meteorologie und Geodynamik* (ZAMG, Wien) for providing access to the data of the European Centre for Medium-Range Weather Forecasts and Arthur Niell for his helpful review.

References

Berg H (1948) Allgemeine Meteorologie. Dümmler Verlag, Bonn

Boehm J, B Werl, H Schuh (2006a) Troposphere mapping functions for GPS and very long baseline interferometry from European Centre for Medium-Range Weather Forecasts operational analysis data. J. Geophys. Res., 111, B02406, doi: 10.1029/2005JB003629

Boehm J, AE Niell, P Tregoning, H Schuh (2006b) The Global Mapping Function (GMF): A new empirical mapping function based on data from numerical weather model data. Geophys. Res. Lett., 33, L07304, doi: 10.1029/2005GL025546

Heiskanen WA, H Moritz (1967) Physical Geodesy. Freeman, San Francisco

Hopfield HS (1969) Two-quartic tropospheric refractivity profile for correcting satellite data, *J. Geophys. Res.*, 74: 4487-4499

Hugentobler U, R Dach, P Fridez, and M Meindl (eds.) (2006) *Bernese GPS Software Version 5.0*, Astronomical Institute, University of Berne

King RW, Y Bock (2006) *Documentation for the GAMIT GPS processing software Release 10.2*, Mass. Inst. of Technol., Cambridge, MA

Lemoine FG, SC Kenyon, JK Factor, RG Trimmer, NK Pavlis, DS Chinn, CM Cox, SM Klosko, SB Luthcke, MH Torrence, YM Wang, RG Williamson, EC Pavlis, RH Rapp, TR Olson (1998) The development of the joint NASA GSFC and the National Imagery and Mapping Agency (NIMA) geopotential model EGM96. NASA/TP-1998-20681, NASA, Greenbelt

MacMillan DS, C Ma (1994) Evaluation of very long baseline interferometry atmospheric modeling improvements. *J. Geophys. Res.*, 99(B1): 637-651

Niell AE (1996) Global mapping functions for the atmosphere delay at radio wavelengths. *J. Geophys. Res.*, 101(B2): 3227-3246

Saastamoinen J (1972) Atmospheric correction for the troposphere and stratosphere in radio ranging of satellites. The use of artificial satellites for geodesy, *Geophys. Monogr. Ser.* 15, Amer. Geophys. Union, 274-251

Tregoning P, TA Herring (2006) Impact of a priori hydrostatic zenith delay errors on GPS estimates of station heights and zenith total delays. *Geophys. Res. Letters*, 33, L23303, doi:10.1029/2006GL027706

Uppala SM, PW Kållberg, AJ Simmons, U Andrae, V da Costa Bechtold, M Fiorino, JK Gibson, J Haseler, A Hernandez, GA Kelly, X Li, K Onogi, S Saarinen, N Sokka, RP Allan, E Andersson, K Arpe, MA Balmaseda, ACM Beljaars, L van de Berg, J Bidlot, N Bormann, S Caires, F Chevallier, A Dethof, M Dragosavac, M Fisher, M Fuentes, S Hagemann, E Hólm, BJ Hoskins, L Isaksen, PAEM Janssen, R Jenne, AP McNally, J-F Mahfouf, J-J Morcrette, NA Rayner, RW Saunders, P Simon, A Sterl, KE Trenberth, A Untch, D Vasiljevic, P Viterbo, and J Woollen (2005) The ERA-40 re-analysis, *Quarterly Journal of the Royal Meteorological Society*, 131, doi:10.1256/qj.04.176, pp. 2961-3012

Johannes Böhm, Paulo Jorge Mendes Cerveira, Harald Schuh,
and Paul Tregoning

The impact of mapping functions for the neutral atmosphere
based on numerical weather models in GPS data analysis

IAG Symposium Series, Vol. 130, Springer-Verlag
edited by Paul Tregoning and Chris Rizos, pp 837-843

2007b

The impact of mapping functions for the neutral atmosphere based on numerical weather models in GPS data analysis

Johannes Böhm, Paulo Jorge Mendes Cerveira, Harald Schuh, and Paul Tregoning

Abstract

Since troposphere modelling is one of the major error sources in the geodetic applications of Global Positioning System (GPS) and Very Long Baseline Interferometry observations, mapping functions have been developed in the last years which are based on data from numerical weather models. This paper presents the first results with the Vienna Mapping Functions 1 (VMF1) implemented in a GPS software package (GAMIT/GLOBK). The analysis of a global GPS network from July 2004 until July 2005 with VMF1 and the Niell Mapping Functions (NMF) shows that station heights can change by more than 10 mm, in particular from December to January in the Antarctic, Japan, the northern part of Europe and the western part of Canada, and Alaska. The application of the VMF1 (instead of NMF) also improves the repeatability of the geodetic results and reduces seasonal signals in the station height time series.

Keywords: Mapping function, GPS, numerical weather model, VMF1

1 Introduction

One of the major error sources in the analyses of Global Positioning System (GPS) and Very Long Baseline Interferometry (VLBI) observations is modelling path delays in the neutral atmosphere of microwave signals transmitted by satellites or emitted from astronomical radio sources. The common concept of troposphere modelling is based on the separation of the path delay, ΔL , into a hydrostatic and a wet part (Davis et al. 1985).

$$(1) \quad \Delta L(e) = \Delta L_h^z \cdot m_h(e) + \Delta L_w^z \cdot m_w(e)$$

In Equation 1, the total delays $\Delta L(e)$ at an elevation angle e are made up of a hydrostatic (index h) and a wet (index w) part, and each of these terms is the product of the zenith delay (ΔL_h^z or ΔL_w^z) and the corresponding mapping function m_h or m_w . These mapping functions,

which are independent of the azimuth of the observation, have been determined for the hydrostatic and the wet part separately by fitting the coefficients a , b , and c of a continued fraction form (Marini 1972) to standard atmospheres (e.g. Chao 1974), to radiosonde data (Niell 1996), or recently to numerical weather models (NWMs) (Niell 2001, Boehm and Schuh 2004). The hydrostatic zenith delays, ΔL_h^z , can be determined from the total pressure p and the station coordinates at a site (Saastamoinen 1973), and the hydrostatic and wet mapping functions are assumed to be known. The wet zenith delays ΔL_w^z are estimated within the least-squares adjustment of the GPS or VLBI observations.

The Vienna Mapping Functions 1 (VMF1), as introduced by Boehm and Schuh (2004) and updated by Boehm et al. (2005), are based on raytracing through the NWMs at an initial elevation angle of 3.3° . It has been shown for VLBI analyses (Boehm et al. 2005) that VMF1 yields significantly better results in terms of baseline length repeatabilities than the Niell Mapping Functions (NMF) (Niell 1996) (which uses an empirical function dependent on only the day of year and station latitude and height) and that its application will influence the terrestrial reference frame (TRF). The investigations presented here show the first GPS results with the VMF1 implemented in a GPS software package (GAMIT/GLOBK) (King and Bock, 2005; Herring, 2005). We use solutions computed with the NMF as a reference because it is most often used in GPS and VLBI analysis, and thus it is the basis for the present realization of the terrestrial reference frame.

Several investigations (e.g., Boehm et al. 2005) have shown that there is no significant station height change resulting from differences between the VMF1 and NMF wet mapping functions. In contrast, there are significant differences between the hydrostatic mapping functions at low elevations which cause apparent station height changes. There exists a "rule of thumb" to estimate the approximate height change from a difference in the hydrostatic mapping function (Niell et al. 2001): *"The change of the station height is approximately one third of the tropospheric delay difference at the lowest elevation included in the analysis. (Station heights increase with increasing mapping functions.)"* This rule of thumb shall be illustrated by one example: Figures 1 and 2 show the hydrostatic delays at 7° elevation calculated using the NMF and VMF1 for station OHI2 (O'Higgins, Antarctica), and the corresponding station heights obtained from GPS analysis, respectively. In January, when the difference between VMF1 and NMF is at a maximum (30 mm), differences of the station heights are also a maximum (10 mm).

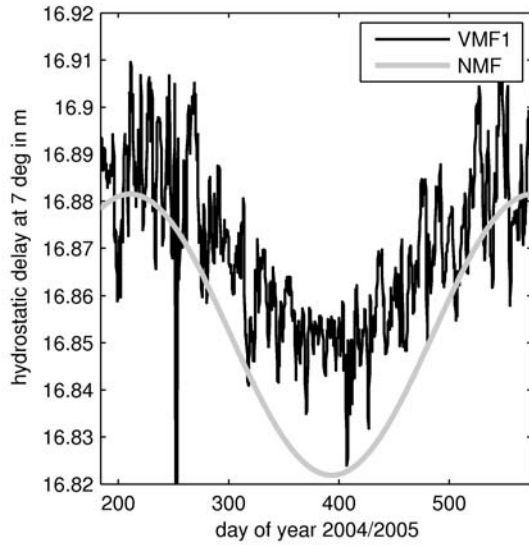


Fig. 1. Hydrostatic delays at 7° elevation determined with NMF and VMF1 at station OHI2 (O'Higgins), Antarctica. There is good agreement between the mapping functions in July and August, but the disagreement reaches ~ 30 mm at 7° elevation in the Antarctic summer (from December through to February).

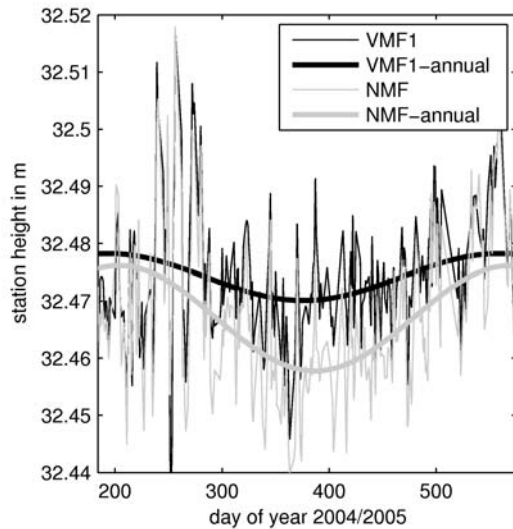


Fig. 2. Station heights of OHI2 determined from GPS with NMF or VMF1 with an elevation cutoff angle of 7°. The annual variation is plotted for both time series. The differences of the hydrostatic delays (Figure 1) are mirrored in the station height differences. The station height difference in January 2005 is about 10 mm, which is approximately one third of the hydrostatic delay difference at 7° elevation. The amplitude of the annual variation becomes significantly smaller when using VMF1 instead of NMF.

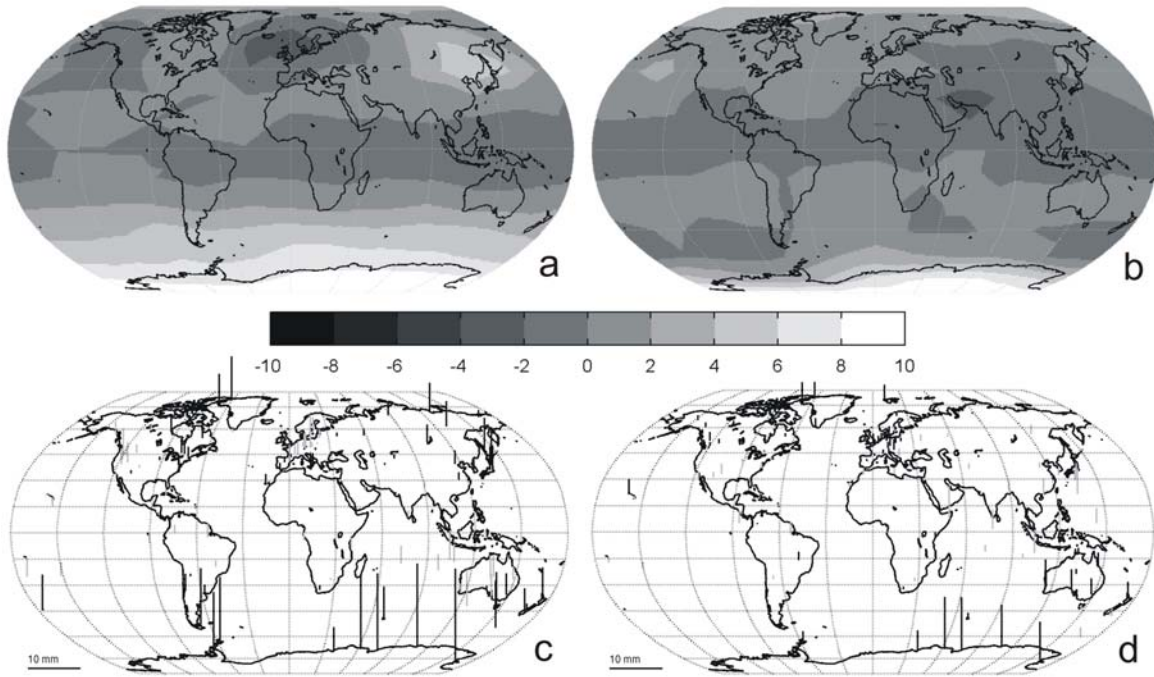


Fig. 3a. GPS station height changes (in mm) simulated from ERA40 data for January 2001 when using VMF1 instead of NMF. From these simulations, large positive station height changes (>10 mm) can be expected for Antarctica and around Japan and negative height changes can be expected for the northern part of Europe. Fig. 3b. GPS station height changes (in mm) simulated from ERA40 data for July 2001 when using VMF1 instead of NMF. In July 2001, there are only relatively small height changes which can be expected in other years, too. Fig. 3c. Station height differences from GPS analysis using either NMF or VMF1 for January 2005. Black bars indicate positive height changes, grey bars negative height changes. It is evident that these analysis data confirm the simulations from ERA40 data for January 2001 (Figure 3a), i.e. positive station height changes can be found in the southern hemisphere and around Japan, and negative station height changes occur at stations in northern Europe, the western part of Canada, and Alaska. Fig. 3d. Station height differences from GPS analysis using either NMF or VMF1 for July 2005. Clearly, these analyses confirm the simulations from ERA40 data for July 2001 (Figure 3b), i.e. the estimated station height changes are moderate compared to January (see Figure 3c).

2 Simulation studies

Based on monthly mean values from 40 years re-analysis data (ERA40) provided by the European Centre for Medium-Range Weather Forecasts (ECMWF) in 2001, differences between the two hydrostatic mapping functions, NMF and VMF1, have been determined on a

global grid (30° in longitude by 15° in latitude) for an elevation angle of 7° . Multiplied by the hydrostatic zenith delay which is taken from the ERA40 data, the hydrostatic delay differences at 7° can be applied to assess the apparent station height changes when using VMF1 instead of NMF with the rule of thumb mentioned above. Figure 3a shows these simulated station height changes (VMF1 minus NMF) for January 2001 with large positive values for stations south of -45° latitude and also for those in Japan and north-eastern China. On the other hand, the changes are negative over the northern part of Europe, the western part of Canada, and Alaska. In contrast, there are hardly any differences in June through August (Figure 3b), indicating that there is a much better agreement between NMF and VMF1 at that time (except for Antarctica). Since there is a clear annual signal in the differences of the mapping functions, it can be expected that the apparent station height changes for 2001 would be very similar in other years. In other words, Figures 3a and 3b show the errors that have been introduced into the estimates of GPS or VLBI station heights that have been obtained previously when using the NMF based on a common assumption for the global weather.

3 Vienna Mapping Functions in the GAMIT software

A global network of more than 100 GPS stations was analysed with the software package GAMIT software Version 10.21 (King and Bock, 2005) applying first the NMF and then the VMF1 mapping functions. We analysed a full year of global observations from July 2004 until July 2005, producing a fiducial-free global network for each day analysed. The elevation cutoff angle was set to 7° and no downweighting of low observations was applied. Atmospheric pressure loading (tidal and non-tidal) (Tregoning and van Dam, 2005) was applied along with ocean tide loading and the IERS2003 solid Earth tide model (IERS Conventions 2003). We estimated satellite orbital parameters, station coordinates, zenith tropospheric delay parameters every 2 hours, and resolved ambiguities where possible. We used ~ 60 sites to transform the fiducial-free networks into the ITRF2000 by estimating 6-parameter transformations (3 rotations, 3 translations) (Herring 2005). For the investigations described below the time series of estimated station heights at 133 sites were used. Each of these sites has more than 300 daily height estimates. The site distribution is shown in Figure 3c.

Amplitudes A and phases do_{y_0} (in terms of day of year) of annual periodic signals were estimated by the method of least-squares for all station heights from the NMF and VMF1 time

series (see Figure 2). Then these sinusoidal functions (Equation 2) were used to calculate the station height differences on 1 January 2005 and 1 July 2005, respectively (Figures 3c,d).

$$(2) \quad h = A \cdot \sin\left(\frac{\text{doy} - \text{doy}_0}{365.25} \cdot 2\pi\right)$$

A comparison of the estimated height differences from GPS with those predicted from the NWMs shows a very high correlation (cf. Figures 3a/3c and Figures 3b/3d). This confirms that the NMF has temporal deficiencies, with a maximum around January, especially at high southern latitudes, for Japan, the northern part of Europe, the western part of Canada, and Alaska.

Figure 4 shows the amplitudes and phases for all 133 GPS stations. (Figure 5 shows amplitudes and phases in Europe for clarity.) Generally, the VMF1 reduced the amplitudes of annual variations on around 50% of sites. However, there is a systematic improvement (reduction of amplitude larger than 5 mm, see Figure 2) at sites situated below 45° S, indicating deficiencies of the NMF at higher southern latitudes. The agreement between the amplitudes and phases when changing from NMF to VMF1 is rather good; however, at some stations, especially in the southern hemisphere and in northern Europe, large discrepancies occur. This may be due to the short time series that has been used in this analysis (only one year). If significant, these changes in amplitudes of annual signals might influence the determination of normal modes of the Earth according to Blewitt (2003).

The standard deviation of the station heights with respect to the sinusoidal functions clearly decreases for almost all stations using the VMF1 compared to NMF (Figure 6). The standard deviation of the daily station heights with regard to the annual signal is smaller for 117 of the 133 stations, and the average relative improvement is about 6%. Thus, using the VMF1 not only changes the terrestrial reference frame but it also improves considerably the precision of the GPS analysis.

The progression from the old NMF to the new mapping functions based on NWMs influences the terrestrial reference frame by changing the heights of some stations - in particular, in Japan and in some regions of the northern hemisphere (Figure 7). Thus, there will be a distortion of the whole frame and rather likely a general shift along the z-axis. As radio-wave techniques play an important role in the realization of the International Terrestrial Reference Frame (ITRF), a significant influence on the next ITRF can be expected if weather-based mapping functions are used in the analysis of the GPS and VLBI observations.

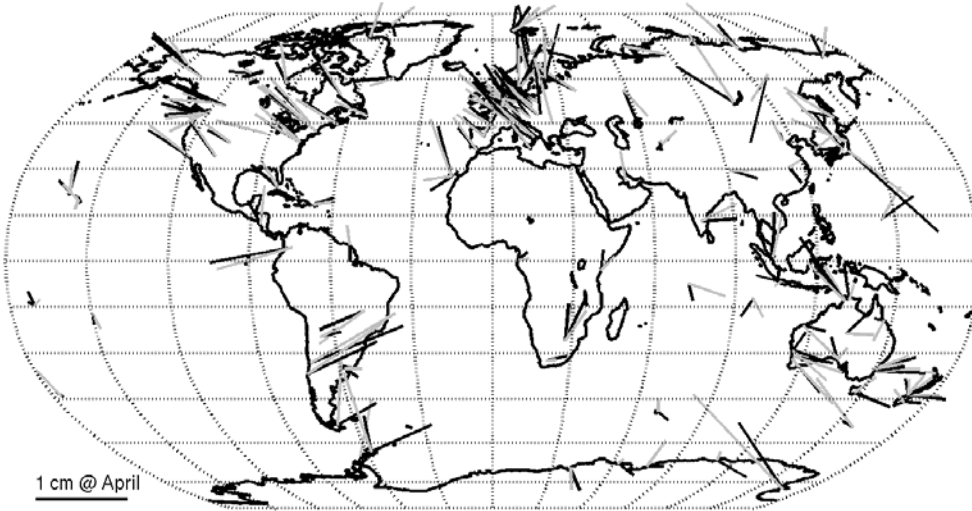


Fig. 4. Amplitudes A and phases doy_0 (see Equation 2) of annual variation in the station height time series determined from GPS analyses using NMF or VMF1. The grey bars correspond to NMF, the black bars to VMF1. The phase angles doy_0 are counted from north (January) to east (April).

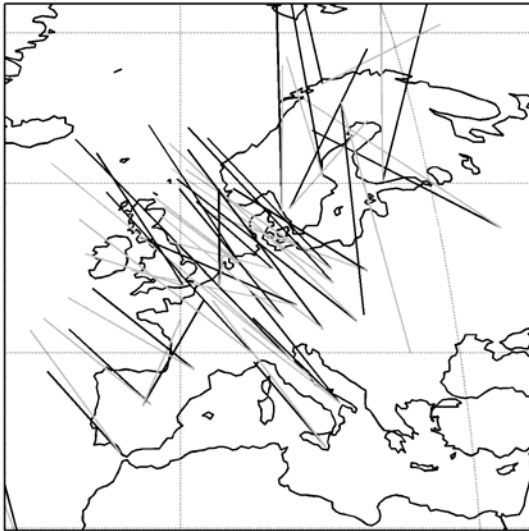


Fig. 5. Amplitudes A and phases doy_0 (see Equation 2) of annual variation in the station height time series determined from GPS analyses using NMF or VMF1 in Europe. The grey bars correspond to NMF, the black bars to VMF1. The phase angles doy_0 are counted from north (January) to east (April).

The results presented here are derived from analyses where no elevation-dependent weighting of the observations has been performed. Very similar results are obtained when such weighting is used, although the influence of the more accurate tropospheric mapping functions is reduced.

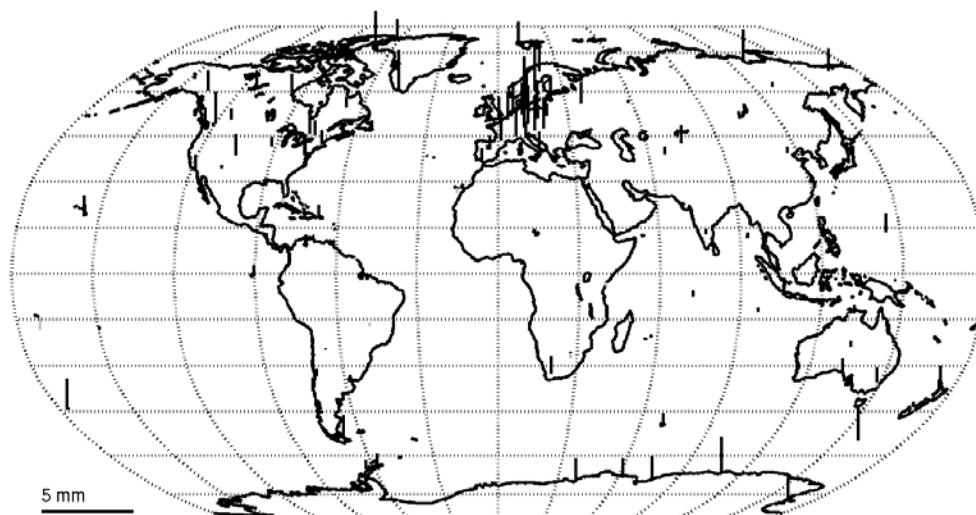


Fig. 6. Difference of standard deviations of the station height time series after removing the annual signal. A clear improvement of the residual station heights is evident when using VMF1 instead of NMF. Black bars indicate improvement with VMF1, grey bars with NMF.

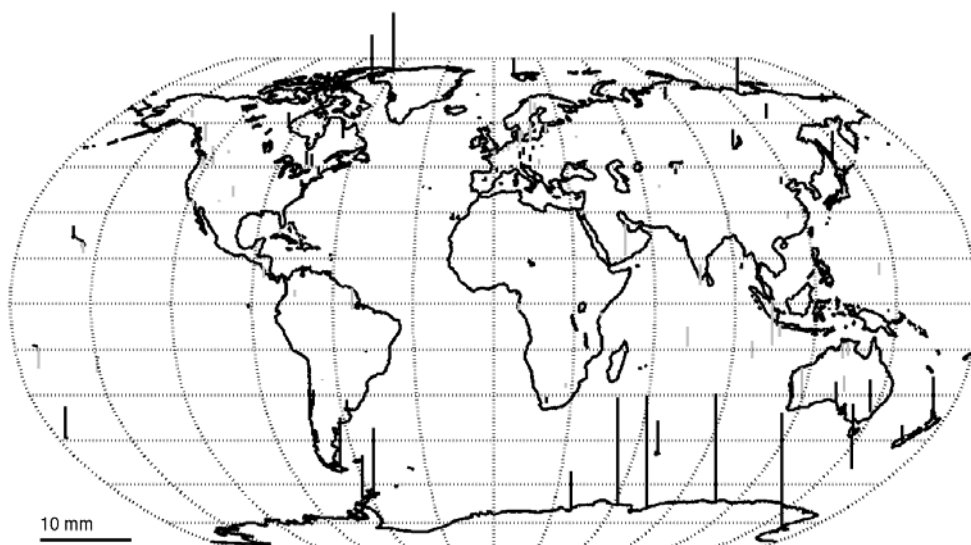


Fig. 7. Yearly mean station height changes when using VMF1 instead of NMF. Black lines indicate increase of station heights, grey lines indicate decrease.

4 Conclusions

For the first time, the Vienna Mapping Functions 1 (VMF1) based on data from a numerical weather model have been applied in global GPS analysis. Significant improvements in the precision of geodetic results are found compared to using the Niell Mapping Function (NMF) based on a very general assumption about the global weather. After removing an annual signal, the standard deviation of the residual station heights decreases for more than 87% of

the stations, and the average relative improvement is about 6% compared to NMF, with values as high as 30% at some stations. Furthermore, the application of the Vienna Mapping Functions 1 will change the terrestrial reference frame by changing station heights. The maximum station height differences (up to 20 mm) when changing from the NMF to VMF1 occur in January, especially in Antarctica, Japan, the northern part of Europe, the western part of Canada, and Alaska.

Acknowledgements

We would like to thank ZAMG in Austria for providing us access to the ECMWF data and the Austrian Science Fund (FWF) (project P16992-N10) for supporting this work. We are also grateful to the IGS for providing the global geodetic data. The inclusion of the VMF1 into the GAMIT software was funded in part by the Fonds National de la Recherche du Luxembourg grant FNR/03/MA06/06. The GPS analyses were computed on the Terrawulf linux cluster belonging to the Centre for Advanced Data Inference at the Research School of Earth Sciences, The Austrian National University.

References

- Blewitt G (2003). Self-consistency in reference frames, geocenter definition, and surface loading of the solid Earth, *Journal of Geophysical Research*, Vol. 108, NO. B2, 2103, doi: 10.129/2002JB002082
- Boehm J, Schuh H (2004). Vienna Mapping Functions in VLBI analyses, *Geophys. Res. Lett.* 31(1):L01603, DOI:10.1029/2003GL018984
- Boehm J, Werl B, Schuh H (2005). Troposphere mapping functions for GPS and VLBI from ECMWF operational analyses data, *Journal of Geophysical Research*, *in press*.
- Chao CC (1974) The troposphere calibration model for Mariner Mars 1971, *JPL Technical Report 32-1587*, NASA JPL, Pasadena CA
- Davis JL, Herring TA, Shapiro II, Rogers AEE, Elgered G (1985). Geodesy by Radio Interferometry: Effects of Atmospheric Modeling Errors on Estimates of Baseline Length, *Radio Science* 20(6):1593-1607
- Herring TA (2005) GLOBK Global Kalman Filter VLBI and GPS analysis program, version 10.1, *Mass. Inst. of Technol.*, Cambridge, MA

King RW, Bock Y (2005). Documentation for the GAMIT GPS processing software Release 10.2, *Mass. Inst. of Technol.*, Cambridge, MA

McCarthy, DD, Petit G (2004). IERS Conventions (2003), IERS Technical Note, No. 32, Verlag des Bundesamtes für Kartographie und Geodäsie

Marini JW (1972). Correction of satellite tracking data for an arbitrary tropospheric profile, *Radio Science*, Vol. 7, No. 2, pp. 223-231

Niell AE (1996). Global mapping functions for the atmosphere delay at radio wavelengths, *J. Geophys. Res.* 101(B2):3227-3246

Niell A.E. (2001). Preliminary evaluation of atmospheric mapping functions based on numerical weather models, *Phys. Chem. Earth*, 26, 475-480

Niell AE, Coster AJ, Solheim FS, Mendes VB, Toor PC, Langley RB, Upham CA (2001). Comparison of Measurements of Atmospheric Wet Delay by Radiosonde, Water Vapor Radiometer, GPS, and VLBI, *Journal of Atmospheric and Oceanic Technology* 18:830-850

Saastamoinen J (1973). Contributions to the Theory of Atmospheric Refraction, Part II, *Bulletin Geodesique*, Vol. 107, pp. 13-34

Tregoning P, van Dam T (2005). Atmospheric pressure loading corrections applied to GPS data at the observation level, *Geophys. Res. Lett.*, 32, L22310, doi:10.1029/2005GL024104

Johannes Böhm and Harald Schuh

Troposphere Gradients from the ECMWF in VLBI analysis

Journal of Geodesy, Vol. 81, No. 6-8, pp 409-421

doi:10.1007/s00190-006-0126-9

2007c

Troposphere gradients from the ECMWF in VLBI analysis

Johannes Böhm and Harald Schuh

Abstract

Modeling path delays in the neutral atmosphere for the analysis of Very Long Baseline Interferometry (VLBI) observations has been improved significantly in the last years by the use of elevation-dependent mapping functions based on data from numerical weather models (NWM). In this paper, we present a fast way of extracting both, hydrostatic and wet, linear horizontal gradients (LHG) for the troposphere from data of the European Centre for Medium-Range Weather Forecasts (ECMWF), as it is realized at the Vienna University of Technology on a routine basis for all stations of the International GNSS Service (IGS) and International VLBI Service for Geodesy and Astrometry (IVS) stations. This approach only uses information about the refractivity gradients at the site vertical but no information from the line-of-sight. VLBI analysis of the CONT02 and CONT05 campaigns as well as all IVS-R1 and IVS-R4 sessions in the first half of 2006 shows that fixing these a priori gradients improves the repeatability for 74% (40 out of 54) of the VLBI baseline lengths compared to fixing zero or constant a priori gradients and improves the repeatability for the majority of baselines compared to estimating 24-hour offsets for the gradients. Only if 6-hour offsets are estimated the baseline length repeatabilities significantly improve, no matter which a priori gradients are used.

Keywords: Troposphere modeling - troposphere gradients - VLBI - ECMWF

1 Introduction

In the analysis of Global Navigation Satellite System (GNSS) and Very Long Baseline Interferometry (VLBI) observations the neutral atmosphere delays ΔL have to be accounted for by either appropriate models or estimation of distinct parameters. The azimuth-independent part of the neutral atmosphere around a station is usually described with elevation-dependent mapping functions $m_h(\epsilon)$ and $m_w(\epsilon)$ for the hydrostatic and wet part, respectively, and the corresponding zenith delays $\Delta L_{h,w}^z$ (Eq. 1) (Davis et al. 1985). While the

hydrostatic zenith delays are determined from the pressure values at the site, the wet zenith delays are estimated in the least-squares adjustment.

$$(1) \quad \Delta L(\alpha, \varepsilon) = \Delta L_h^z m_h(\varepsilon) + \Delta L_w^z m_w(\varepsilon) + m_g(\varepsilon) [G_n \cos(\alpha) + G_e \sin(\alpha)]$$

North and east gradients, G_n and G_e , which describe the azimuth-dependent part of the neutral atmosphere (Davis et al. 1993), are used to determine the gradient at the azimuth α of the observation which is then mapped with the gradient mapping function $m_g(\varepsilon)$ to the elevation of the observation. Although different models are available for the gradient mapping function (e.g. Chen and Herring 1997), we use the simple equation by MacMillan (1995) with the wet mapping function (Eq. 2).

$$(2) \quad m_g(\varepsilon) = m_w(\varepsilon) \cdot \cot(\varepsilon)$$

Some analysts use a priori hydrostatic gradients which are either constant in time (e.g. from the Data Assimilation Office (DAO) at the NASA Goddard Space Flight Center (Schubert et al. 1994) as used by MacMillan and Ma (1997)) or determined at 6-hour time intervals from the tilting of the 200 hPa pressure level (Niell 2001). However, as wet gradients are usually estimated in VLBI and GNSS analysis and the partial derivatives for the hydrostatic and wet gradients are (nearly) identical, the influence of a priori hydrostatic gradients on the geodetic parameters is rather small as will be illustrated in Section 3.

It has been shown by Niell (2006) by comparisons with radiosonde data that the accuracy of the Vienna Mapping Function 1 (VMF1, Boehm et al. 2006) is better than 10 mm at 5° elevation, which corresponds to a station height accuracy better than 2 mm if the cutoff elevation angle is set to 5°. Similarly, a gradient error of 0.1 mm is equivalent to a delay error of about 10 mm at 5° elevation and corresponds to a horizontal station error of about 1 mm. In Section 2, we consider a fast way of extracting the total, i.e. hydrostatic and wet, gradients from data provided by the European Centre for Medium-Range Weather Forecasts (ECMWF), and in Section 3 we use these gradients in the analysis of VLBI observations. Although the precision of these gradients is in most cases worse than 0.1 mm, they provide a useful tool for investigations on asymmetries in tropospheric delays and gradients in particular.

2 Determination of linear horizontal gradients from the ECMWF

2.1 Linear horizontal gradients (LHG) from the vertical profile at the site

In their derivation of wet gradients, Davis et al. (1993) assume that the linear horizontal gradients G can be determined for a specific azimuth α if the refractivity gradient $dN_\alpha(z)$ is known for the neutral atmosphere at any height z above the site and that $dN_\alpha(z)$ is valid at any horizontal distance d around the vertical profile (Fig. 1 and description there). Eq. 3 shows how the gradients G_α can be obtained from a NWM as the vertical integral of the refractivity gradient $dN_\alpha(z)$ weighted with height (z) assuming linear horizontal gradients of refractivity around the site.

$$(3) \quad G_\alpha = 10^{-6} \cdot \int_{z=0}^{\infty} dN_\alpha(z) \cdot z \cdot dz$$

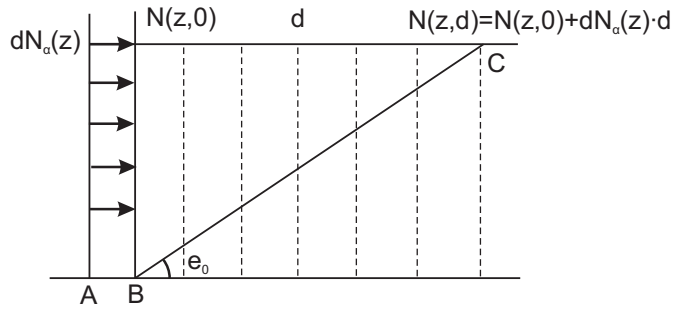


Fig 1 The derivation of the linear horizontal gradients (LHG) is based on the assumption that the gradients of refractivity $dN_\alpha(z)$ at height z and azimuth α are valid at any horizontal distance d around the site vertical. Two adjacent profiles (at A and B, in our study 0.25° apart) with pressure, temperature, and humidity are needed for LHG to determine the gradients of refractivity along the site vertical. On the other hand, tens of profiles are needed for VMF2 (see Section 2.2) in each direction (dashed lines) to derive the refractivity along the slant path (through C). Obviously, LGH suffers from the assumption that the gradients of refractivity between A and B are supposed to continue to any other location which might be hundreds of kilometers away. (The curvature of the Earth is neglected in this figure.)

From the ECMWF, refractivity profiles can be downloaded for selected sites with a horizontal resolution of 0.25° (less than 30 km) and a time resolution of 6 hours. Consequently, three profiles per site are extracted: the one closest to the site, one profile towards north and one

profile towards east. Then, the refractivity gradients $dN(z)$ can be determined by differencing the profiles, and the north and east gradients, G_n and G_e , can be calculated with Eq. 3. Fig. 2 shows the weighted refractivity gradients $dN_n(z) \cdot z$ towards north at Kokee Park on 10 October 2002 at 0:00 UT. It is evident that the hydrostatic gradients are primarily caused by refractivity gradients at about 8 km to 20 km, whereas the wet gradients are due to gradients of the wet refractivity in the first few kilometers above the stations.

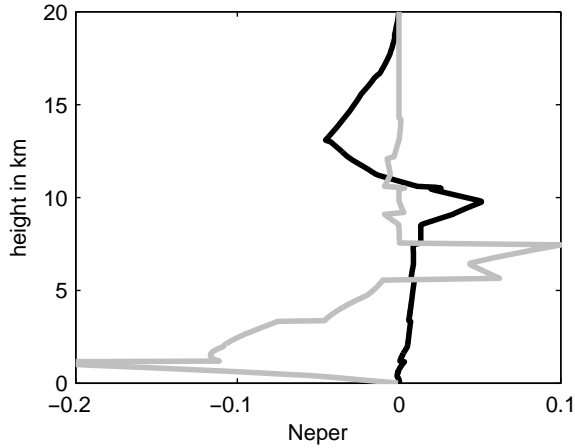


Fig. 2 Weighted (with height) refractivity gradients ($dN(z) \cdot z$) towards north at Kokee Park (Hawaii, U.S.A.) on 10 October 2002 at 0:00 UT. The black line shows the hydrostatic, the grey line the wet gradients.

This approach (Eq. 3), which will be referred to as LHG in the following, has the advantage that only information from the site vertical is needed. Thus, if (e.g.) the ECMWF would add fields with the derivatives of the geopotential, temperature, and humidity towards north and east to their analysis pressure level fields, the quantities expressed by Eq. 3 could be easily provided, too, and the gradients would be available globally and with the computational resolution inherent to the ECMWF fields.

2.2 Comparison with the azimuth-dependent Vienna Mapping Functions (VMF2) for CONT02

For CONT02, a continuous VLBI campaign over 15 days in October 2002 organized by the International VLBI Service for Geodesy and Astrometry (IVS) (Schlueter et al. 2002), Boehm et al. (2005) determined azimuth-dependent Vienna Mapping Functions (VMF2), i.e. the VMF provided every 30° in azimuth at 6-hour time intervals. Around each site, hundreds of profiles with pressure, temperature, and humidity were downloaded (cf. dashed lines in Fig.

1), and then the hydrostatic and wet mapping functions were determined for an (initial) elevation angle e_0 of 3.3° . These mapping function values were used to derive the coefficients 'a' of the continued fraction form for the mapping functions (Niell 1996) taking the best empirical equations for the coefficients 'b' and 'c' available (Boehm et al. 2006). However, this approach is very time consuming, especially as far as the extraction of hundreds of profiles around each site is concerned. Thus, the application of LHG as derived from Eq. 3 is compared with VMF2 during CONT02 to evaluate whether LHG could be used instead of VMF2 without a significant loss of accuracy.

Fig. 1 shows that the LHG are based on the assumption that the linear horizontal gradients of refractivity between the profiles at A and B continue to any other part of the atmosphere that is passed through by the signals, even if it is hundreds of kilometers apart. But the average gradients between the profiles at A and C are generally smaller than those between the profiles at A and B, and the reduction of the average gradients is smaller at lower heights z . Since the effective height for the hydrostatic gradients is larger than for the wet gradients (Fig. 2), the corresponding reduction factor is larger for the hydrostatic than for the wet gradients. Comparing VMF2 and LHG for CONT02, we empirically found the factors 0.53 (hydrostatic) and 0.71 (wet) which we then applied to the hydrostatic and wet gradients derived from Eq. 3. Additionally, all wet gradients were cut at a maximum value of ± 1 mm to exclude extreme wet gradients, which can also be caused by extreme wet gradients between the profiles at A and B that do not continue to C.

Table 1 Total delay differences in mm at 5° elevation between LHG and VMF2 for CONT02. The median standard deviation is at about 15 mm, the maximum standard deviation occurs at Hartebeesthoek with 43 mm for the north gradient.

	bias north [mm]	bias east [mm]	std.dev. north [mm]	std.dev. east [mm]
Algonquin Park (Canada)	-10	0	10	10
Gilmore Creek (Alaska, U.S.A.)	-5	5	24	13
Westford (U.S.A)	-11	1	25	14
Kokee Park (Hawaii, U.S.A.)	-1	15	19	34
Onsala (Sweden)	-8	-1	12	10
NyÅlesund (Norway)	1	-5	12	8
Wettzell (Germany)	2	-6	18	12
Hartebeesthoek (South Africa)	0	2	43	19

Table 1 shows that the median standard deviation of the total delay differences at 5° elevation between VMF2 and LHG is about 15 mm for CONT02, and that the largest standard deviation is found for the north gradient at Hartebeesthoek with 43 mm. On average, the variance between LHG and VMF2 is about one fourth of the power that is in the gradient time series. We do not present the separation between hydrostatic and wet gradients here because the accuracy of the total gradients is essential for VLBI analysis if no residual gradients are estimated.

Exemplarily, Fig. 3 shows the total north gradients at Kokee Park during CONT02 as LHG and as derived from VMF2, both expressed as asymmetric delays at 5° elevation. Furthermore, the mean hydrostatic gradients from the DAO weather model (Schubert et al. 1994) as used by MacMillan and Ma (1997) are displayed.

While VMF2 provides gradients (strictly speaking, mapping functions) every 30° in azimuth, i.e. 12 values per epoch, the standard approach for the LHG only consists of north and east gradients. Comparisons show that the standard deviation in azimuth between VMF2 and LHG is less than 4 mm at 5° elevation for the hydrostatic part for all eight CONT02 stations. For the wet part the standard deviation is less than 10 mm, except for Kokee Park with 14 mm and Hartebeesthoek with 23 mm.

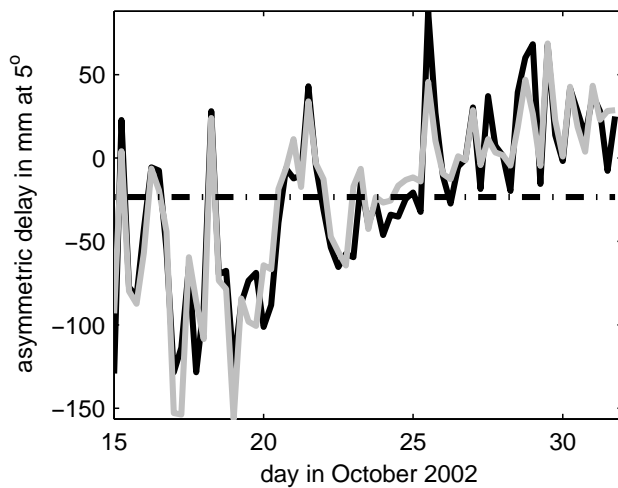


Fig. 3 North gradients expressed as asymmetric delays at 5° elevation at Kokee Park during CONT02. The solid black line shows the reduced linear horizontal gradients LHG, the solid grey line VMF2, and the dash-dot line the mean (hydrostatic) gradient derived from the DAO weather model.

3 Linear horizontal gradients in VLBI analysis

While the LHG have been compared with VMF2 only during CONT02 (see Section 2.2), we show their application in VLBI analysis for CONT02 and CONT05, another continuous VLBI campaign over 15 days in September 2005, and for all IVS-R1 and IVS-R4 sessions from January to July 2006. We compare nine different solutions in terms of baseline length repeatabilities, i.e. standard deviations of the baseline lengths with respect to a regression polynomial of first order. Three different a priori gradients are used: zero gradients ('N'), mean hydrostatic gradients from DAO ('D') (Macmillan and Ma 1997), and total linear horizontal gradients (LHG) as described in Section 2 ('G'). These three a priori gradients are combined with three different approaches of estimating residual gradients: no estimation of residual gradients ('0'), gradients estimated as 24-hour offsets ('24'), and gradients estimated as 6-hour offsets ('6'). In the least-squares analysis of VLBI observations, the estimated gradients are constrained to their a priori values with a standard deviation of 0.5 mm.

Free network solutions (with No-Net-Rotation and No-Net-Translation conditions) have been determined for each 24-hour session of CONT02 and CONT05 with the software package OCCAM v6 (Titov et al. 2004) applying ocean loading corrections (Scherneck 1991) using the ocean tide model GOT00.2 (Ray 1999), atmosphere loading corrections (Petrov and Boy 2004), and corrections for thermal deformations of the radio telescopes (Haas et al. 1999). The azimuth-independent part of the neutral atmosphere has been modelled with VMF1 (Boehm et al. 2006).

In the following we analyse the reduction of variance of baseline length repeatabilities with respect to 'G0', i.e. we take the squared repeatabilities for the baselines with a certain setup and subtract the squared repeatabilities from 'G0'. Only those baselines were considered with more than 15 estimates. Fig. 4 shows the median reduction of variance in mm^2 (over all baselines) with the solution 'G0' as reference. It is evident that fixing the gradients to LHG is better than fixing the gradients to zero values ('N0') or constant values ('D0'). This improvement slightly decreases if gradients are estimated once per 24-hour session ('N24' or 'D24'). As even the majority of baselines with the solution 'G24' is slightly worse than with 'G0', we can conclude that (at least for the VLBI data treated here) there is no benefit from estimating 24-hour gradients in addition to using LHG as a priori gradients. On the other hand, there is a further median improvement if the gradients are estimated every 6 hours no matter which a priori gradients are applied ('N6', 'D6', or 'G6').

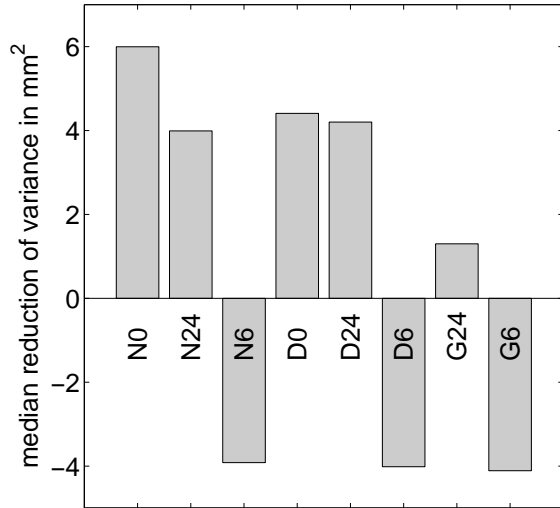


Fig. 4 Median reduction of variance in mm^2 for all CONT02 and CONT05 as well as all IVS-R1 and IVS-R4 sessions in the first half of 2006 with the solution 'G0' as reference. Positive values show an improvement with 'G0', i.e. the repeatability of the majority of baselines improves.

Fig. 5 shows the reduction of variance for the individual baselines when fixing the gradients to LHG ('G0') instead of using no gradients at all ('N0'). It is evident that the repeatability of the majority (40 out of 54) of the baselines improves with LHG ('G0'). Thus, LHG could be used if the network geometry or the observation density is not good enough to allow for the estimation of 6-hour gradients, e.g. for sparse VLBI networks. However, it has to be mentioned that most of the degraded baselines in Fig. 5 include Kokee Park (white bars). In particular, there is no improvement for the typical IVS-Intensive baselines from Kokee Park to Wettzell and Wettzell to Tsukuba. This might partly be due to the rather poor agreement of the east gradients between VMF2 and LHG at this site (Table 1), but more likely to the insufficient quality of the numerical weather model at this site in general.

The comparison between the solutions 'G0' and 'N0' shows (Fig. 5) that the largest improvement from 'N0' to 'G0' can be found for the baselines with TIGO, Concepción, i.e. when using LHG as a priori gradients. The situation for TIGO is extraordinary as on the other hand (not shown here) the improvement from 'G0' to 'G6' is again largest for the baselines with TIGO, i.e. when estimating gradients as 6-hour offsets. This implies that for TIGO the LHG is superior to constant or zero gradients, but nevertheless the estimation of gradients at TIGO is necessary to absorb other residual gradients (or instrumental errors) as well. Fig. 6 shows the total east gradients at TIGO as determined from the ECMWF (LHG) and as estimated with VLBI during CONT05.

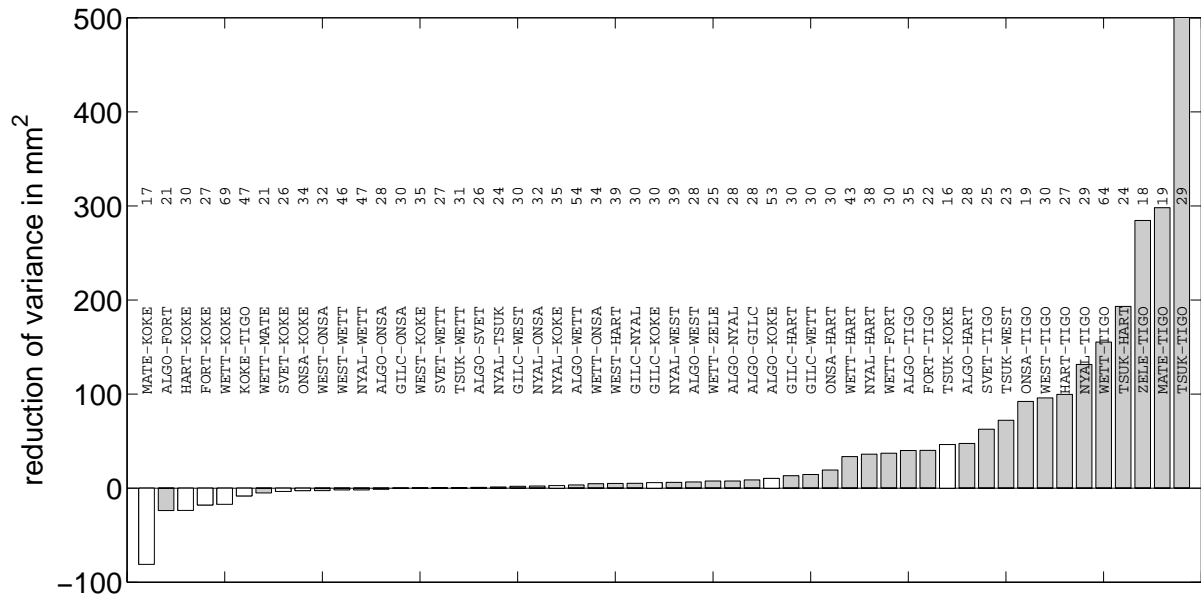


Fig. 5 Reduction of variance in mm^2 of the baseline length repeatabilities for all CONT02, CONT05, and IVS-R1 and IVS-R4 baselines from January to July 2006 when using LHG ('G0') instead of no gradients at all ('N0'). Positive reduction values correspond to an improvement when doing the 'G0' solutions. The number of estimates per baseline is also given in the upper part of the plot, and baselines including Kokee Park are shown as white bars.

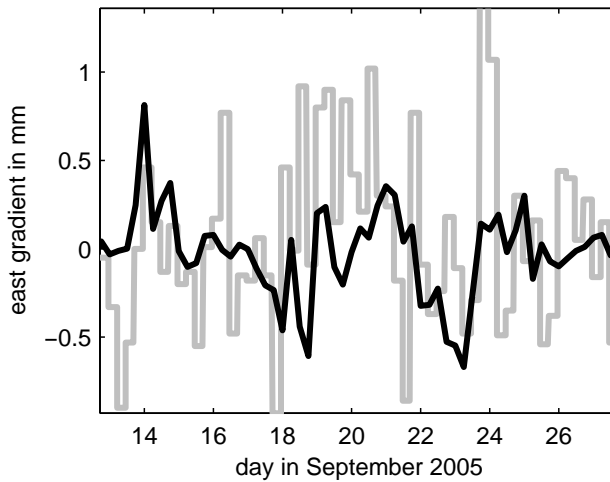


Fig. 6 East gradients in mm as determined from ECMWF (black) and as estimated as 6-hour offsets during CONT05 for station TIGO, Concepción (Chile).

4 Conclusions and outlook

Comparisons for CONT02 demonstrate that the simple concept of linear horizontal gradients (LHG) agrees with the concept of the azimuth-dependent VMF2 at the 0.2 mm level with

maximum standard deviations of up to 0.4 mm at certain sites. Although VMF2 will be affected by errors in the numerical weather models and – to a minor extent – by deficiencies in the model, too, future investigations will deal with the provision of VMF2 (or a similar approach using spherical harmonics as described by Boehm and Schuh (2001)) on a routine basis for the most important geodetic sites.

It has been shown for VLBI analysis that there is no benefit if fixing the gradients to LHG as long as gradients are estimated as 6-hour offsets. However, the LHG can improve the analysis of VLBI sessions for which gradients cannot be estimated because of the poor network geometry or the small number of observations. It also needs to be investigated whether and to which extent the estimation of gradients accounts for other (instrumental) errors, too.

LHG are provided for all VLBI, GPS, and DORIS sites for which the coefficients of VMF1 are available (see <http://www.hg.tuwien.ac.at/~ecmwf1>) starting with 1 January 2006. These time-series can not only be used in VLBI (and GNSS or DORIS) analysis, but they can also be applied for comparisons with gradients determined with space geodetic techniques.

Acknowledgements

We are grateful to the IVS for providing the VLBI observations and to the Zentralanstalt für Meteorologie und Geodynamik (ZAMG), Vienna, for granting us access to the data from the ECMWF. This work is supported by the Austrian Science Fund (FWF) within project P18404-N10.

References

Boehm J, Schuh H (2001) Spherical Harmonics as a Supplement to Global Tropospheric Mapping Functions and Horizontal Gradients, Proceedings of the 15th Working Meeting on European VLBI for Geodesy and Astrometry, ed. by Behrend D and Rius A, Institut d'Estudis Espacials de Catalunya, Barcelona, Spain, pp. 143-148

Boehm J, Ess M, Schuh H (2005) Asymmetric Mapping Functions for CONT02 from ECMWF, Proceedings of the 17th Working Meeting on European VLBI for Geodesy and Astrometry, ed. by Vennebusch M and Nothnagel A, Istituto di Radioastronomia, Noto, Italy, pp. 64-68

Boehm J, Werl B, Schuh H (2006) Troposphere mapping functions for GPS and very long baseline interferometry from European Centre for Medium-Range Weather Forecasts operational analysis data, *J. Geophys. Res.*, 111, B02406, doi:10.129/2005JB003629

Chen G, Herring TA (1997) Effects of atmospheric azimuthal asymmetry on the analysis from space geodetic data, *J. Geophys. Res.*, 102(B9):20489-20502

Davis JL, Herring TA, Shapiro II, Rogers AEE, Elgered G (1985), *Geodesy by Radio Interferometry: Effects of Atmospheric Modelling Errors on Estimates of Baseline Length*, *Radio Science*, 20(6):1593-1607

Davis JL, Elgered G, Niell AE, Kuehn CE (1993) Ground-based measurements of the gradients in the 'wet' radio refractivity of air, *Radio Science*, 28(6):1003-1018

Haas R, Nothnagel A, Schuh H, Titov O (1999) Explanatory Supplement to the Section 'Antenna Deformation' of the IERS Conventions (1996), DGFI Report No. 71, Deutsches Geodätisches Forschungsinstitut (DGFI), Munich, pp. 26-29

MacMillan DS (1995) Atmospheric gradients from very long baseline interferometry observations, *Geophys. Res. Lett.*, 22(9):1041-1044

MacMillan DS, Ma C (1997) Atmospheric gradients and the VLBI terrestrial and celestial reference frames, *Geophys. Res. Letters*, 24(4):453-456

Niell (1996) Global mapping functions for the atmosphere delay at radio wavelengths, *J. Geophys. Res.*, 101(B2):3227-3246

Niell AE (2001) An a priori Hydrostatic Gradient Model for Atmospheric Delay, *Proceedings of the 15th Working Meeting on European VLBI for Geodesy and Astrometry*, ed. by Behrend D and Rius A, Institut d'Estudis Espacials de Catalunya, Barcelona, Spain, pp. 133-136

Niell AE (2006) Interaction of Atmosphere Modeling und Analysis Strategy, *IVS 2006 General Meeting Proceedings*, ed. by Behrend D, and Baver KD, NASA/CP-2006

Petrov L, Boy JP (2004) Study of the atmospheric pressure loading signal in VLBI observations, *J. Geophys. Res.*, 109, No. B03405, doi:10.1029/2003JB002500

Ray R (1999) A Global Ocean Tide Model From TOPEX/Poseidon Altimetry/GOT99.2 - NASA/TM-1999-209478, Goddard Space Flight Center/NASA, Greenbelt

Scherneck HG (1991) A parameterized solid earth tide model and ocean tide loading effects for global geodetic baseline measurements, *Geophys. J. Int.*, 106:677-694

Schlueter W, Himwich E, Nothnagel A, Vandenberg NR, Whitney A (2002) IVS and Its Important Role in the Maintenance of the Global Reference Systems, *Advances in Space Research*, 30(2):145-150

Schubert SD, Rood RB, Pfaendtner J (1994) An assimilated data set for earth science applications, Bull. Amer. Meteor. Soc., 74:2331-2342

Titov O, Tesmer V, Boehm J (2004) OCCAM v. 6.0 software for VLBI data analysis, International VLBI Service for Geodesy and Astrometry 2004 General Meeting Proceedings, ed. by Vandenberg NR and Baver KD, NASA/CP-2004-212255

Appendix A:**K. Snajdrova, J. Böhm, P. Willis, R. Haas, and H. Schuh****Multi-technique comparison of tropospheric zenith delays derived during the CONT02 campaign****Journal of Geodesy, doi:10.1007/s00190-005-0010-z, 2005****Abstract**

In October 2002, 15 continuous days of Very Long Baseline Interferometry (VLBI) data were observed in the Continuous VLBI 2002 (CONT02) campaign. All eight radio telescopes involved in CONT02 were co-located with at least one other space-geodetic technique, and three of them also with a Water Vapor Radiometer (WVR). The goal of this paper is to compare the tropospheric zenith delays observed during CONT02 by VLBI, Global Positioning System (GPS), Doppler Orbitography Radiopositioning Integrated by Satellite (DORIS) and WVR and to compare them also with operational pressure level data from the European Centre for Medium-Range Weather Forecasts (ECMWF). We show that the tropospheric zenith delays from VLBI and GPS are in good agreement at the 3–7mm level. However, while only small biases can be found for most of the stations, at Kokee Park (Hawaii, USA) and Westford (Massachusetts, USA) the zenith delays derived by GPS are larger by more than 5mm than those from VLBI. At three of the four DORIS stations, there is also a fairly good agreement with GPS and VLBI (about 10 mm), but at Kokee Park the agreement is only at about 30mm standard deviation, probably due to the much older installation and type of DORIS equipment. This comparison also allows testing of different DORIS analysis strategies with respect to their real impact on the precision of the derived tropospheric parameters. Ground truth information about the zenith delays can also be obtained from the ECMWF numerical weather model and at three sites using WVR measurements, allowing for comparisons with results from the space-geodetic techniques. While there is a good agreement (with some problems mentioned above about DORIS) among the space-geodetic techniques, the comparison with WVR and ECMWF is at a lower accuracy level. The complete CONT02 data set is sufficient to derive a good estimate of the actual precision and accuracy of each geodetic technique for applications in meteorology.

Appendix B**V. Tesmer, J. Böhm, R. Heinkelmann, H. Schuh****Effect of different tropospheric mapping functions on the TRF, CRF and position time-series estimated from VLBI****Journal of Geodesy, doi:10.1007/s00190-006-0126-9, 2007****Abstract**

This paper compares estimated terrestrial reference frames (TRF) and celestial reference frames (CRF) as well as position time-series in terms of systematic differences, scale, annual signals and station position repeatabilities using four different tropospheric mapping functions (MF): The NMF (Niell Mapping Function) and the recently developed GMF (Global Mapping Function) consist of easy-to-handle stand-alone formulae, whereas the IMF (Isobaric Mapping Function) and the VMF1 (Vienna Mapping Function 1) are determined from numerical weather models. All computations were performed at the Deutsches Geodätisches Forschungsinstitut (DGFI) using the OCCAM 6.1 and DOGS-CS software packages for Very Long Baseline Interferometry (VLBI) data from 1984 until 2005. While it turned out that CRF estimates only slightly depend on the MF used, showing small systematic effects up to 0.025 mas, some station heights of the computed TRF change by up to 13 mm. The best agreement was achieved for the VMF1 and GMF results concerning the TRFs, and for the VMF1 and IMF results concerning scale variations and position time-series. The amplitudes of the annual periodical signals in the time-series of estimated heights differ by up to 5 mm. The best precision in terms of station height repeatability is found for the VMF1, which is 5–7% better than for the other MFs.

Appendix C

J. Böhm and Harald Schuh

Spherical Harmonics as a Supplement to Global Tropospheric Mapping Functions and Horizontal Gradients

In: D. Behrend and A. Rius (Eds.): Proceedings of the 15th Working Meeting on European VLBI for Geodesy and Astrometry, Institut d'Estudis Espacials de Catalunya, Consejo Superior de Investigaciones Científicas, Barcelona, Spain, 2001

Abstract

Global mapping functions are used to map the tropospheric zenith path delays down to the path delays at certain elevations. Recently, horizontal tropospheric gradients have also been applied to account for azimuthal asymmetries of the path delays. Anyway, there are still deficiencies when combining the elevation-dependent mapping functions and horizontal gradients to model the tropospheric path delays. Spherical Harmonics to describe those deficiencies are tested by solving for the respective coefficients. Tests show that some combinations of Spherical Harmonics yield slightly better results than applying the standard approach of global mapping function plus gradient.

GEOWISSENSCHAFTLICHE MITTEILUNGEN

Bisher erschienen:

- Heft 1 Kolloquium der Assistenten der Studienrichtung Vermessungswesen. 1970 - 1973, Dezember 1973.
- Heft 2 EGGER-PERDICH-PLACH-WAGENSOMMERER, Taschenrechner HP 45 und HP 65, Programme und Anwendungen im Vermessungswesen. 1. Auflage, März 1974, Special Edition in English, Juli 1974, 2. verbesserte Auflage, November 1974.
- Heft 3 Kolloquium der Assistenten der Studienrichtung Vermessungswesen 1973 - 1974, September 1974.
- Heft 4 EGGER-PALFINGER-PERDICH-PLACH-WAGENSOMMERER, Tektronix-Tischrechner TEK 31, Programmbibliothek für den Einsatz im Vermessungswesen, November 1974.
- Heft 5 K.LEDERSTEGE, Die horizontale Isostasie und das isostatische Geoid, Februar 1975.
- Heft 6 F.REINHART, Katalog von FK4 Horrebow-Paaren für Breiten von +30 bis +60, Oktober 1975.
- Heft 7 Arbeiten aus dem Institut für Höhere Geodäsie, Wien, Dezember 1975.
- Heft 8 Veröffentlichungen des Instituts für Photogrammetrie zum XIII. Internationalen Kongreß für Photogrammetrie in Helsinki 1976, Wien, Juli 1976.
- Heft 9 W.PILLEWIZER, Felsdarstellung aus Orthophotos, Wien, Juni 1976.
- Heft 10 PERDICH-PLACH-WAGENSOMMERER, Der Einsatz des programmierbaren Taschenrechners Texas Instruments SR-52 mit Drucker PC100 in ingenieurgeodätischen Rechentechnik, Wien, Mai 1976.
- Heft 11 Kolloquium der Assistenten der Studienrichtung Vermessungswesen 1974 - 1976, November 1976.
- Heft 12 Kartographische Vorträge der Geodätischen Informationstage 1976, Wien, Mai 1977.
- Heft 13 Veröffentlichung des Instituts für Photogrammetrie anlässlich des 80. Geburtstages von Prof.Dr.h.c.K.Neumaier, Wien, Januar 1978.
- Heft 14 L.MOLNAR, Self Checking Analytical Relative Orientation and Strip Formation, Wien, Dezember 1978.
- Heft 15 Veröffentlichung des Instituts für Landesvermessung anlässlich des 80. Geburtstages von Prof.Dr.Alois Bavir, Wien, Januar 1979.
- Heft 16 Kolloquium der Assistenten der Studienrichtung Vermessungswesen 1976 - 1978, Wien, November 1979.
- Heft 17 E.VOZIKIS, Die photographische Differentialumbildung gekrümmter Flächen mit Beispielen aus der Architekturbildmessung, Wien, Dezember 1979.

- Heft 18 Veröffentlichung des Instituts für Allgemeine Geodäsie anlässlich des 75. Geburtstages von Prof.Dipl.Ing.Dr.F.Hauer, Die Höhe des Großglockners, Wien, 1981.
- Heft 19 H.KAGER, Bündeltriangulation mit indirekt beobachteten Kreiszentren, Wien, April 1981.
- Heft 20 Kartographische Vorträge der Geodätischen Informationstage 1980, Wien, Mai 1982.
- Heft 21 Veröffentlichung des Instituts für Kartographie anlässlich des 70. Geburtstages von Prof.Dr.Wolfgang Pillewizer: Glaziologie und Kartographie, Wien, Dezember 1982.
- Heft 22 K.TEMPFLI, Genauigkeitsschätzung digitaler Höhenmodelle mittels Spektralanalyse, Wien, Mai 1982.
- Heft 23 E.CSAPLOVICS, Interpretation von Farbinfrarotbildern, Wien, November 1982.
- Heft 24 J.JANSA, Rektifizierung von Multispektral-Scanneraufnahmen - Entwicklung und Erprobung eines EDV-Programms, Wien, Mai 1983.
- Heft 25 Zusammenfassung der Diplomarbeiten, Dissertationen und Habilitationen an den geodätischen Instituten der TU Wien, Wien, November 1984.
- Heft 26 T.WUNDERLICH, Die voraussetzungsfreie Bestimmung von Refraktionswinkeln, Wien, August 1985.
- Heft 27 G.GERSTBACH (Hrsg.), Geowissenschaftliche/geotechnische Daten in Landinformationssystemen - Bedarf und Möglichkeiten in Österreich, Juni 1986.
- Heft 28 K.NOVAK, Orientierung von Amateuraufnahmen ohne Paßpunkte, Wien, August 1986.
- Heft 29 Veröffentlichung des Instituts für Landesvermessung und Ingenieurgeodäsie, Abt. Ingenieurgeodäsie, anlässlich des 80. Geburtstages von Prof.Dipl.Ing.Dr.F.Hauer, Wien, Oktober 1986.
- Heft 30 K.-H.ROCH, Über die Bedeutung dynamisch ermittelter Parameter für die Bestimmung von Gesteins- und Gebirgseigenschaften, Wien, Februar 1987.
- Heft 31 G. HE, Bildverbesserung mittels digitaler Filterung, Wien, April 1989.
- Heft 32 F.SCHLÖGELHOFER, Qualitäts- und Wirtschaftlichkeitsmodelle für die Ingenieurphotogrammetrie, Wien, April 1989.
- Heft 33 G.GERSTBACH (Hrsg.), Geowissenschaftliche/geotechnische Daten in Landinformationssystemen - Datenbestände und Datenaustausch in Österreich, Wien, Juni 1989.
- Heft 34 F.HOCHSTÖGER, Ein Beitrag zur Anwendung und Visualisierung digitaler Geländemodelle, Wien, Dezember 1989.
- Heft 35 R.WEBER, Lokale Schwerefeldmodellierung unter Berücksichtigung spektraler Methoden zur Geländereduktion, Wien, April 1990.

- Heft 36 o.Prof.Dr.Hans Schmid zum 70. Geburtstag. Veröffentlichung der Abteilung für Landesvermessung, Wien, Oktober 1990.
- Heft 37 G.GERSTBACH, H.P.HÖLLRIEGL und R.WEBER, Geowissenschaftliche Informationsbörse - Eine Nachlese zu GeoLIS II, Wien, Oktober 1990.
- Heft 38 R.ECKER, Rastergraphische Visualisierungen mittels digitaler Geländemodelle, Wien, August 1991.
- Heft 39 Kartographische Forschungen und Anwendungsorientierte Entwicklungen, herausgegeben von W.Stams und F.Kelnhofer zum 80. Geburtstag von Prof.Dr.W.Pillewizer, Wien, Juli 1991.
- Heft 39a W.RIEGER, Hydrologische Anwendungen des digitalen Geländemodelles, Wien, Juli 1992.
- Heft 40 K.STEINNOCHER, Methodische Erweiterungen der Landnutzungs-klassifikation und Implementierung auf einem Transputernetzwerk, Wien, Juli 1994.
- Heft 41 G.FORKERT, Die Lösung photogrammetrischer Orientierungs- und Rekonstruktionsaufgaben mittels allgemeiner kurvenförmiger Elemente, Wien, Juli 1994.
- Heft 42 M.SCHÖNER, W.SCHÖNER, Photogrammetrische und glaziologische Untersuchungen am Gâsbre (Ergebnisse der Spitzbergenexpedition 1991), Wien, Mai 1996.
- Heft 43 M.ROIC. Erfassung von nicht signalisierten 3D-Strukturen mit Video-theodoliten, Wien, April 1996.
- Heft 44 G.RETSCHER, 3D-Gleiserfassung mit einem Multisensorsystem und linearen Filterverfahren, Wien, April 1996.
- Heft 45 W.DAXINGER, Astrogravimetrische Geoidbestimmung für Ingenieurprojekte, Wien, Juli 1996.
- Heft 46 M.PLONER, CCD-Astrometrie von Objekten des geostationären Ringes, Wien, November 1996.
- Heft 47 Zum Gedenken an Karl Killian "Ingenieur" und "Geodät" 1903-1991, Veröffentlichung der Fachgruppe Geowissenschaften, Wien, Februar 1997.
- Heft 48 A.SINDHUBER, Ergänzung und Fortführung eines digitalen Landschaftsmodelles mit multispektralen und hochauflösenden Fernerkundungsaufnahmen, Wien, Mai 1998.
- Heft 49 W.WAGNER, Soil Moisture Retrieval from ERS Scatterometer Data, Wien, Dezember 1998.
- Heft 50 R.WEBER, E.FRAGNER (Editoren), Prof.Bretterbauer, Festschrift zum 70.Geburtstag, Wien, Juli 1999.
- Heft 51 Ch.ÖHRENER, A Similarity Measure for Global Image Matching Based on The Forward Modeling Principle, Wien, April 1999.
- Heft 52 M.LECHTHALER, G.GARTNER, Per Aspera ad Astra, Festschrift für Fritz Kelnhofer zum 60. Geburtstag, Wien, Jänner 2000.
- Heft 53 F.KELNHOFER, M.LECHTHALER, Interaktive Karten (Atlanten) und Multimedia - Applikationen, Wien, März 2000.

- Heft 54 A.MISCHKE, Entwicklung eines Videotheodolit-Meßsystems zur automatischen Richtungsmessung von nicht signalisierten Objektpunkten, Wien, Mai 2000
- Heft 55 Veröffentlichung des I.P.F. anlässlich der Emeritierung von Prof.Dr. Peter Waldhäusl, Wien.
- Heft 56 F.ROTTENSTEINER, Semi-automatic Extraction of Buildings Based on Hybrid Adjustment Using 3D Surface Models and Management of Building Data in a TIS, Wien, Juni 2001.
- Heft 57 D.LEGENSTEIN, Objektrekonstruktion aus perspektiven Bildern unter Einbeziehung von Umrisslinien, Wien, Mai 2001.
- Heft 58 F.KELNHOFER, M.LECHTHALER und K.BRUNNER (Hrsg.), Telekartographie und Location Based Services, Wien, Jänner 2002.
- Heft 59 K.BRETTERBAUER, Die runde Erde eben dargestellt: Abbildungslehre und sphärische Kartennetzentwürfe, Wien, 2002.
- Heft 60 G.GARTNER, Maps and the Internet 2002, Wien 2002.
- Heft 61 L.DORFFNER, Erzeugung von qualitativ hochwertigen 3D Photomodellen für Internetbasierte Anwendungen mit besonderem Augenmerk auf Objekte der Nahbereichsphotogrammetrie, Wien, Jänner 2002.
- Heft 62 CHMELINA, Wissensbasierte Analyse von Verschiebungsdaten im Tunnelbau Wien 2002
- Heft 63 A.NIESSNER, Qualitative Deformationsanalyse unter Ausnutzung der Farbinformation, Wien 2002
- Heft 64 K.BRETTERBAUER; R.WEBER, A Primer of Geodesy for GIS-Users, Wien im Herbst 2003
- Heft 65 N.PFEIFER, 3D Terrain Models on the basis of a triangulation, Wien, Jänner 2002.
- Heft 66 G.GARTNER (Hrsg), Location Based Services & Telecartography, Wien, 2004
- Heft 67 I.KABASHI, Gleichzeitig-gegenseitige Zenitwinkelmessung über größere Entfernungen mit automatischen Zielsystemen, Wien, 2004
- Heft 68 J.BÖHM, Troposphärische Laufzeitverzögerungen in der VLBI, Wien 2004
- Heft 69 R.WEBER, W.SCHLÜTER, U.SCHREIBER, O. TITOV
Evolving Space Geodesy Techniques (EGS XXVII General Assembly, Nice, France, 2002), Wien 2004
- Heft 70 G. WEINWURM, Amalthea's Gravity Field and its Impact on a Spacecraft Trajectory, Wien 2004
- Heft 71 Forschungsgruppe Ingenieurgeodäsie, Festschrift anlässlich des 65. Geburtstages von Herrn o.Univ.Prof.Dr.-Ing. Heriber Kahmen, Wien 2005
- Heft 72 A. REITERER, A Knowledge-Based Decision System for an On-Line Video-Theodolite-Based Multisensor System, Wien 2005
- Heft 73 M. HABERLER, Einsatz von Fuzzy Methoden zur Detektion konsistenter Punktbewegungen, Wien 2005
- Heft 74 G. GARTNER, Location Based Services & Telecartography, Proceedings of the Symposium 2005, Wien 2005

- Heft 75 Th. HOBIGER, VLBI as a tool to probe the ionosphere, Wien 2006
- Heft 76 E. KLAFFENBÖCK, Troposphärische Laufzeitverzögerung von GNSS-Signalen – Nutzen aktiver Referenzstationsnetze für die Meteorologie, Wien 2006
- Heft 76a P.J. MENDES-CERVEIRA, Tidal and non-tidal contributions to surface loading processes on station coordinates, Wien 2006
- Heft 78 G. KOSTOV, G. BOURDA, L. FERNANDEZ, T. KONDO, Research Projects at IGG – Reports, Wien 2007
- Heft 79 J. BÖHM, A. PANY, H. SCHUH (Editors), Proceedings of the 18th European VLBI for Geodesy and Astrometry Working Meeting, 12-13 April 2007, Wien 2007